

# **An Effective Model of the Retinoic Acid Induced HL-60 Differentiation Program**

Ryan Tasseff, Holly A. Jensen, Johanna Congleton<sup>†</sup>, Wei Dai, Katherine Rogers, Adithya Sagar, Rodica P. Bunaciu<sup>†</sup>, Andrew Yen<sup>†</sup>, and Jeffrey D. Varner\*

Robert Frederick Smith School of Chemical and Biomolecular Engineering and <sup>†</sup>Department of Biomedical Sciences, Cornell University, Ithaca NY 14853

**Running Title:** Effective modeling of HL-60 differentiation

**To be submitted:** ?

\*Corresponding author:

Jeffrey D. Varner,

Professor, Robert Frederick Smith School of Chemical and Biomolecular Engineering,  
244 Olin Hall, Cornell University, Ithaca NY, 14853

Email: jdv27@cornell.edu

Phone: (607) 255 - 4258

Fax: (607) 255 - 9166

## **Abstract**

In this study, we present an effective model All-Trans Retinoic Acid (ATRA)-induced differentiation of HL-60 cells. The model describes a key architectural feature of ATRA-induced differentiation, positive feedback between an ATRA-inducible signalsome complex involving many proteins including Vav1, a guanine nucleotide exchange factor, and the activation of the mitogen activated protein kinase (MAPK) cascade. The model, which was developed by integrating logical rules with kinetic modeling, was significantly smaller than previous models. However, despite its simplicity, it captured key features of ATRA induced differentiation of HL-60 cells. We identified an ensemble of effective model parameters using measurements taken from ATRA-induced HL-60 cells. Using these parameters, model analysis predicted that MAPK activation was bistable as a function of ATRA exposure. Conformational experiments supported ATRA-induced bistability. These findings, combined with other literature evidence, suggest that positive feedback is central to a diversity of cell fate programs.

## **1 Introduction**

2 Understanding the architecture of differentiation programs is an important therapeutic  
3 challenge. Differentiation induction chemotherapy (DIC), using agents such as the vita-  
4 min A derivative all-trans retinoic acid (ATRA), is a promising approach for the treatment  
5 of many cancers (1–3). For example, ATRA treatment induces remission in 80–90% of  
6 promyelocytic leukemia (APL) PML-RAR $\alpha$ -positive patients (4), thereby transforming a  
7 fatal diagnosis into a manageable disease. However, remission is sometimes not durable  
8 and relapsed cases exhibit emergent ATRA resistance (5, 6). To understand the basis of  
9 this resistance, we must first understand the ATRA-induced differentiation program. To-  
10 ward this challenge, lessons learned in model systems, such as the lineage-uncommitted  
11 human myeloblastic cell line HL-60, could inform our analysis of the more complex dif-  
12 ferentiation programs occurring in patients. Patient derived HL-60 leukemia cells have  
13 been a durable experimental model since the 1970's to study differentiation (7). HL-60  
14 undergoes cell cycle arrest and either myeloid or monocytic differentiation following stim-  
15 ulation; ATRA induces G1/G0-arrest and myeloid differentiation in HL-60 cells, while 1,25-  
16 dihydroxy vitamin D3 (D3) induces arrest and monocytic differentiation. Commitment to  
17 cell cycle arrest and differentiation requires approximately 48 hr of treatment, during which  
18 HL-60 cells undergo two division cycles.

19 Sustained mitogen-activated protein kinase (MAPK) activation is a defining feature of  
20 ATRA-induced HL-60 differentiation. ATRA drives sustained MEK-dependent activation  
21 of the Raf/MEK/ERK pathway, leading to arrest and differentiation (8). MEK inhibition re-  
22 sults in the loss of ERK and Raf phosphorylation, and the failure to arrest and differentiate  
23 (9). ATRA (and its metabolites) are ligands for the hormone activated nuclear transcrip-  
24 tion factors retinoic acid receptor (RAR) and retinoid X receptor (RXR) (10). RAR/RXR  
25 activation is necessary for ATRA-induced Raf phosphorylation (9), and the formation of  
26 an ATRA-inducible signalsome complex at the membrane which drives MAPK activation

27 through a yet to be identified kinase activity. While the makeup of the signalsome com-  
28 plex is not yet known, we do know that it is composed of Src family kinases Fgr and Lyn,  
29 PI3K, c-Cbl, Slp76, and KSR, as well as IRF-1 transcription factors (11–15). Signalsome  
30 formation and activity is driven by ATRA-induced expression of CD38 and the putative  
31 heterotrimeric Gq protein-coupled receptor BLR1 (16, 17). BLR1, identified as an early  
32 ATRA (or D3)-inducible gene using differential display (18), is necessary for MAPK ac-  
33 tivation and differentiation (17), and is also involved with signalsome activity. Studies  
34 of the BLR1 promoter identified a 5' 17bp GT box approximately 1 kb upstream of the  
35 transcriptional start that conferred ATRA responsiveness (17). Members of the BLR1  
36 transcriptional activator complex, e.g. NFATc3 and CREB, are phosphorylated by ERK,  
37 JNK or p38 MAPK family members suggesting positive feedback between the signalsome  
38 and MAPK activation (19). BLR1 overexpression enhanced Raf phosphorylation and ac-  
39 celerated terminal differentiation, while Raf inhibition reduced BLR1 expression and dif-  
40 ferentiation (20). BLR1 knock-out cells failed to activate Raf or differentiate in the pres-  
41 ence of ATRA (20). Interestingly, both the knockdown or inhibition of Raf, also reduced  
42 BLR1 expression and functional differentiation (20). Thus, the expression of signalsome  
43 components e.g., BLR1 was Raf dependent, while Raf activation depended upon the sig-  
44 nalsome. A recent computational study of ATRA-induced differentiation in HL-60 cells  
45 suggested that the BLR1-MAPK positive feedback circuit was sufficient to explain ATRA-  
46 induced sustained MAPK activation, and the expression of a limited number of functional  
47 differentiation markers (21). Model analysis also suggested that Raf was the most distinct  
48 of the MAPK proteins. However, this previous study developed and analyzed a complex  
49 model, thus leaving open the critical question of what is the minimal positive feedback  
50 circuit required to drive ATRA-induced differentiation.

51 In this study, we explored this question using a minimal mathematical model of the  
52 key architectural feature of ATRA induced differentiation of HL-60 cells, namely positive

53 feedback between an ATRA-inducible signalsome complex and MAPK activation. The  
54 ATRA responsive signalsome-MAPK circuit was then used to drive a downstream gene  
55 expression program which encoded for the expression of functional differentiation mark-  
56 ers. The effective model used a novel framework which integrated logical rules with ki-  
57 netic modeling to describe gene expression and protein regulation, while largely relying  
58 upon biophysical parameters from the literature. This formulation significantly reduced  
59 the size and complexity of the model compared to the previous study of Tasseff et al.,  
60 while increasing the breadth of the biology described (21). The effective model, despite  
61 its simplicity, captured key features of ATRA induced differentiation of HL-60 cells. Model  
62 analysis predicted the bistability of MAPK activation as a function of ATRA exposure; con-  
63 formational experiments supported ATRA-induced bistability. Model simulations were also  
64 consistent with measurements of the influence of MAPK inhibitors, and the failure of BLR1  
65 knockout cells to differentiate when exposed to ATRA. Lastly, we showed by through im-  
66 munoprecipitation studies, that the guanine nucleotide exchange factor Vav1 is potentially  
67 a new ATRA-inducible member of the signalsome complex. Taken together, these findings  
68 when combined with other literature evidence, suggested that positive feedback architec-  
69 tures are central to differentiation programs generally, and necessary for ATRA-induced  
70 differentiation.

71 **Results**

72 We constructed an effective model of ATRA-induced HL-60 differentiation which described  
73 signaling and gene expression events following the addition of ATRA (Fig. 1). The model  
74 connectivity was developed from literature and the studies presented here (Table 1). We  
75 decomposed the ATRA program into three modules; a signal initiation module that sensed  
76 and transformed the ATRA signal into activated cRaf-pS621 and the ATRA-RXR/RAR  
77 (Trigger) signals (Fig. 1A); a signal integration module that controlled the expression of  
78 upstream transcription factors given cRaf-pS621 and activated Trigger signals (Fig. 1B);  
79 and a phenotype module which encoded the expression of functional differentiation mark-  
80 ers from the ATRA-inducible transcription factors (Fig. 1C). Each component of these  
81 modules was described by a mRNA and protein balance equation. Additionally, the sig-  
82 nal initiation module also described the abundance of activated species e.g., Trigger and  
83 cRaf-pS621 whose values were derived from unactivated Trigger and cRaf protein levels.  
84 Lastly, because the population of HL-60 cells was dividing (at least before ATRA-induced  
85 cell cycle arrest), we also considered a dilution term in all balance equations. The sig-  
86 nal initiation module contained nine differential equations, while the signal integration and  
87 phenotype modules were collectively encoded by 54 differential equations. Model param-  
88 eters were taken literature (Table 2), or estimated from experimental data using heuristic  
89 optimization (see materials and methods).

90 The signal initiation module recapitulated sustained signalsome and MAPK activation  
91 following exposure to  $1\mu\text{M}$  ATRA (Fig. 2A-B). An ensemble of effective model param-  
92 eters was estimated by minimizing the difference between simulations and time-series  
93 measurements of BLR1 mRNA and cRaf-pS621 following the addition of  $1\mu\text{M}$  ATRA. We  
94 focused on the S621 phosphorylation site of cRaf since enhanced phosphorylation at  
95 this site is a defining characteristic of sustained MAPK activation in HL-60. The effective  
96 model captured both ATRA-induced BLR1 expression (Fig. 2A) and sustained phospho-

97 phosphorylation of cRaf-pS621 (Fig. 2B) in a growing population of HL-60 cells. Together, the  
98 reinforcing positive feedback between the signalsome and MAPK led to sustained activation  
99 over multiple cellular generations. However, the effective model failed to capture the  
100 decline of BLR1 message after 48 hr of ATRA exposure. This suggested that we captured  
101 the logic leading to the onset of differentiation, but failed to describe program shutdown.  
102 Next, we tested the response of the signal initiation module to different ATRA dosages.

103 The signal initiation model was bistable with respect to ATRA induction (Fig. 2C-D).  
104 Phaseplane analysis predicted two stable steady-states when ATRA was present below  
105 a critical threshold, and only a single steady-state above the threshold (Fig. 2C). In the  
106 lower stable state, neither the signalsome nor cRaf-pS621 were present (thus, the differ-  
107 entiation program was deactivated). However, at the high stable state, both the signal-  
108 some and cRaf-pS621 were present, allowing for sustained activation and differentiation.  
109 Interestingly, when ATRA was above a critical threshold, only the activated state was ac-  
110 cessible (Fig. 2D). To test these findings, we first identified the ATRA threshold. We  
111 exposed HL-60 cells to different ATRA concentrations for 72 hr (Fig. 2E). Morphological  
112 changes associated with differentiation were visible for ATRA  $\geq$  0.25  $\mu$ M, suggesting the  
113 critical ATRA threshold was near this concentration. Next, we conducted ATRA washout  
114 experiments to determine if activated cells remained activated in the absence of ATRA.  
115 HL-60 cells locked into an activated state remained activated following ATRA withdraw-  
116 (Fig. 3). This sustained activation resulted from reinforcing feedback between the sig-  
117 nalsome and the MAPK pathway. Thus, following activation, if we inhibited or removed  
118 elements from the signal initiation module we expected the signalsome and MAPK signals  
119 to decay. We simulated ATRA induced activation in the presence of kinase inhibitors, and  
120 without key circuit elements. Consistent with experimental results using multiple MAPK  
121 inhibitors, ATRA activation in the presence of MAPK inhibitors lowered the steady-state  
122 value of signalsome (Fig. 3A). In the presence of BLR1, the signalsome and cRaf-pS621

signals were maintained following ATRA withdraw (Fig. 3B, gray). On the other hand, BLR1 deletion removed the ability of the circuit to maintain a sustained MAPK response following the withdraw of ATRA (Fig. 3B, blue). Lastly, washout experiments in which cells were exposed to  $1\mu\text{M}$  ATRA for 24 hr, and then transferred to fresh media without ATRA, confirmed the persistence of the self sustaining activated state for up to 144 hr (Fig. 3C). Thus, these experiments confirmed that reinforcing positive feedback likely drives the ATRA-induced differentiation program. Next, we analyzed the ATRA-induced downstream gene expression program following signalsome and cRaf activation.

The signal integration and phenotype modules described ATRA-induced gene expression in wild-type HL-60 cells (Fig. 4). The signal initiation module produced two outputs, activated Trigger and cRaf-pS621 which drove the expression of ATRA-induced transcription factors, which then in turn activated the phenotypic program. In particular, Trigger (a surrogate for the RAR $\alpha$ /RXR transcriptional complex) regulated the expression of the transcription factors CCATT/enhancer binding protein  $\alpha$  (C/EBP $\alpha$ ), PU.1, and Egr-1. In turn, these transcription factors, in combination with cRaf-pS621, regulated the expression of downstream phenotypic markers such as CD38, CD11b or p47Phox. We assembled the connectivity of the signal integration and phenotypic programs driven by Trigger and cRaf-pS621 from literature (Table 1). We estimated the parameters for the signal initiation, and phenotype modules from steady-state and dynamic measurements of transcription factor and phenotypic marker expression following the addition of ATRA (22–25). However, the bulk of the model parameters were taken from directly from literature (26) and were not estimated in this study (see materials and methods). The model simulations captured the time dependent expression of CD38 and CD11b following the addition ATRA (Fig. 4A), and the steady-state for signal integration and phenotypic markers (Fig. 4B). Lastly, we used the *predicted* values of the p21 and E2F protein abundance to estimate a black-box model of ATRA-induced G0 arrest (Fig. 5). The phenotype module predicted p21

149 expression significantly increased and E2F expression decreased, in response to ATRA  
150 exposure (Fig. 5A). We then used the ratio of these values in a polynomial model to cal-  
151 culate the fraction of HL-60 cells in G0 arrest following the addition of ATRA (Fig. 5B). The  
152 third-order polynomial model captured the trend in measured G0-arrest values as a func-  
153 tion of time, and was robust to uncertainty in the measured data (Fig. 5B, gray). Taken  
154 together, the output of the signal integration and phenotypic modules was consistent with  
155 time-series and steady-state measurements, thereby validating the assumed molecular  
156 connectivity. Moreover, outputs from the phenotype module described the trend in ATRA-  
157 induced G0 cell cycle arrest. Next, we explored which nodes and interactions between  
158 nodes in the signal integration module most influenced the system response.

159 The Gfi-1 and PPARg proteins were important regulators of ATRA-induced signal in-  
160 tegration and phenotypic change (Fig. 6). We conducted pairwise gene knockout simula-  
161 tions in the signal integration and phenotype modules to estimate which nodes controlled  
162 the processing of the Trigger and cRaF-S621 signals. The difference between the sys-  
163 tem state with and without the gene knockouts (encoded as a normalized state displace-  
164 ment matrix) was decomposed using Singular Value Decomposition (SVD). A panel of  
165 ten parameter sets was sampled, and the average normalized displacement matrix was  
166 decomposed. The first six modes (approximately 36% of the total) described >95% of the  
167 gene knockout variance, with the most important components of these modes being the  
168 Gfi-1 and PPARg proteins, and to a lesser extent PU.1, C/EBPa and AP1 (Fig. 6A).  
169 To better understand which protein-DNA connections were important, we simulated the  
170 pairwise deletion of interactions between these proteins and their respective regulatory  
171 targets. SVD decomposition of the normalized state displacement matrix assembled from  
172 the pairwise connection deletions, suggested the first six modes (approximately 26% of  
173 the total) accounted for >90% of the variance. Globally, the most sensitive interactions  
174 controlled p21 and p47Phox expression, markers for cell-cycle arrest and reactive oxygen

175 formation phenotypic axes activated following ATRA addition (Fig. 6B). Analysis of the  
176 modes suggested the action of PPARg, Gfi-1 and C/EBPa were consistently important  
177 over multiple target genes. The connection knockout analysis also revealed robustness  
178 in the network. For example, no pair of deletions qualitatively changed the expression of  
179 regulators such as PU.1, Oct1, Oct4 or PPARg. Thus, the expression of these species  
180 was robust to disturbance in the connectivity. To better understand the combined influ-  
181 ence of the PPARg and Gfi-1 deletions, we computed the fold change in the protein levels  
182 in the single ( $Gfi-1^{-/-}$  or  $PPARg^{-/-}$ ) and double ( $Gfi-1^{-/-}$  and  $PPARg^{-/-}$ ) mutants for  
183 the best fit parameter set (Fig. 7). Deletion of Gfi-1 led to a 2-4 fold increase in EGR-1,  
184 CD11b and C/EBPa expression, and a  $>8$  fold increase in PU.1 abundance (Fig. 7,blue).  
185 On the other hand, deletion of PPARg led to  $>8$  fold downregulation of CD38, p21, IRF1  
186 and OCT1 (Fig. 7,red). Both knockouts slightly increased E2F expression, but neither  
187 influenced the expression of p47Phox. The double mutant was qualitatively similar to the  
188 combined behavior of the two single mutant cases. Taken together, Gfi-1 and PPARg  
189 controlled the cell-cycle arrest and receptor signaling axes, with PPARg regulating CD38,  
190 IRF1 and p21 expression while Gfi-1 controlled CD11b expression. These simulations  
191 suggested deletion of PPARg and Gfi-1 would not interfere with reactive oxygen forma-  
192 tion, but would limit the ability of HL-60 cells to arrest. However, this analysis did not  
193 give insight into which components upstream of the signal initiation module were impor-  
194 tant. Toward this question, we explored the composition and regulation of the signalsome  
195 complex by experimentally interrogating a panel of possible Raf interaction partners.

196 The composition of the signalsome, and the kinase ultimately responsible for medi-  
197 ating ATRA-induced Raf activation is currently unknown. To explore this question, we  
198 conducted immunoprecipitation and subsequent Western blotting to identify physical in-  
199 teractions between Raf and 19 putative interaction partners. A panel of 19 possible Raf  
200 interaction partners (kinases, GTPases, scaffolding proteins etc) was constructed based

upon known signaling pathways. We did not consider the most likely binding partner, the small GTPase RAS, as previous studies have ruled it out in MAPK activation in HL-60 cells (20, 27). Total Raf was used as a bait protein for the immunoprecipitation studies. Interrogation of the Raf interactome suggested Vav1 was involved with ATRA-induced initiation of MAPK activity (Fig. 8). Western blot analysis using total Raf and pS621 Raf specific antibodies confirmed the presence of the bait protein, total and phosphorylated forms, in the immunoprecipitate (Fig. 8A). Of the 19 proteins sampled, Vav1, Src, CK2, Akt, and 14-3-3 precipitated with Raf, suggesting a direct physical interaction was possible. However, only the associations between Raf and Vav1 and Raf and Src were ATRA-inducible (Fig. 8). Furthermore, the Vav1 and Src associations were correlated with pS621 Raf abundance in the precipitate. Others proteins e.g., CK2, Akt and 14-3-3, generally bound Raf regardless of phosphorylation status or ATRA treatment. The remaining 14 proteins were expressed in whole cell lysate (Fig. 8B), but were not detectable in the precipitate of Raf IP. Treatment with the Raf kinase inhibitor GW5074 following ATRA exposure reduced the association of both Vav1 with Raf and Src with Raf (Fig. 8), although the signal intensity for Src was notably weak. However, GW5074 did not influence the association of CK2 or 14-3-3 with Raf, further demonstrating their independence from Raf phosphorylation. Interestingly, the Raf-Akt interaction qualitatively increased following treatment with GW5074; however, it remained unaffected by treatment with ATRA. Src family kinases are known to be important in myeloid differentiation (28) and their role in HL-60 differentiation has been investigated elsewhere (11). Given the existing work and variable reproducibility in the context of the Raf immunoprecipitate, we did not investigate the role of Src further in this study. Taken together, the immunoprecipitation and GW5074 results implicated Vav1 association to be correlated with Raf activation following ATRA-treatment. Previous studies demonstrated that a Vav1-Slp76-Cbl-CD38 complex plays an important role in ATRA-induced MAPK activation and differentiation of HL-60 cells (13). Here we

227 did not observe direct interaction of Raf with Cbl or Slp76; however, this complex could  
228 be involved upstream. Next, we considered the effect of the Raf kinase inhibitor GW5074  
229 on functional markers of ATRA-induced growth arrest and differentiation.

230 Inhibition of Raf kinase activity modulated MAPK activation and differentiation mark-  
231 ers following ATRA exposure (Fig. 8D-F). ATRA treatment alone statistically significantly  
232 increased the G1/G0 percentage over the untreated control, while GW5074 alone had a  
233 negligible effect on the cell cycle distribution (Fig. 8D). Surprisingly, the combination of  
234 GW5074 and ATRA statistically significantly increased the G1/G0 population ( $82 \pm 1\%$ )  
235 compared with ATRA alone ( $61 \pm 0.5\%$ ). Increased G1/G0 arrest following the combined  
236 treatment with GW5074 and ATRA was unexpected, as the combination of ATRA and the  
237 MEK inhibitor (PD98059) has been shown previously to decrease ATRA-induced growth  
238 arrest (8). However, growth arrest is not the sole indication of functional differentiation.  
239 Expression of the cell surface marker CD11b has also been shown to coincide with HL-60  
240 cells myeloid differentiation (29). We measured CD11b expression, for the various treat-  
241 ment groups, using immuno-fluorescence flow cytometry 48 hr post-treatment. As with  
242 G1/G0 arrest, ATRA alone increased CD11b expression over the untreated control, while  
243 GW5074 further enhanced ATRA-induced CD11b expression (Fig. 8E). GW5074 alone  
244 had no statistically significant effect on CD11b expression, compared with the untreated  
245 control. Lastly, the inducible reactive oxygen species (ROS) response was used as a func-  
246 tional marker of differentiated neutrophils (16). We measured the ROS response induced  
247 by the phorbol ester 12-O-tetradecanoylphorbol-13-acetate (TPA) using flow cytometry.  
248 Untreated cells showed no discernible TPA response, with only  $7.0 \pm 3.0\%$  ROS induction  
249 (Fig. 8F). Cells treated with ATRA had a significantly increased TPA response,  $53 \pm 7\%$   
250 ROS induction 48 hr post-treatment. Treatment with both ATRA and GW5074 statistically  
251 significantly reduced ROS induction ( $22 \pm 0.6\%$ ) compared to ATRA alone. Interestingly,  
252 Western blot analysis did not detect a GW5074 effect on ATRA-induced expression of

253 p47Phox, a required upstream component of the ROS response (Fig. 8F, bottom). Thus,  
254 the inhibitory effect of GW5074 on inducible ROS might occur downstream of p47Phox  
255 expression. However, the ROS producing complex is MAPK dependent, therefore it is  
256 also possible that GW5074 inhibited ROS production by interfering with MAPK activation  
257 (in which case the p47Phox marker might not accurately reflect phenotypic conversion  
258 and differentiation).

259 **Discussion**

260 In this study, we presented an effective model of ATRA-inducible differentiation of HL-60  
261 cells. The model consisted of three modules: a signal initiation module that sensed and  
262 transformed the ATRA signal into activated cRaf-pS621 and the ATRA-RXR/RAR (Trig-  
263 ger) signals; a signal integration module that controlled the expression of upstream tran-  
264 scription factors given cRaf-pS621 and activated Trigger signals; and a phenotype mod-  
265 ule which encoded the expression of functional differentiation markers from the ATRA-  
266 inducible transcription factors. The model described the transcription and translation of  
267 genes in each module, and signaling events in each module in a growing population of  
268 HL-60 cells. Model parameters were taken from literature, however, unknown coefficients  
269 that appear in the promoter logic models were estimated from protein measurements in  
270 HL-60 cells following ATRA exposure. Despite its simplicity, the effective model captured  
271 key features of the ATRA induced differentiation such as sustained MAPK activation, and  
272 bistability with respect to ATRA exposure. The model also described the expression of  
273 upstream transcription factors which regulated the expression of differentiation markers.  
274 Lastly, analysis of the response of the model to perturbations identified Gfi-1 and PPARg  
275 as master regulators of ATRA-induced differentiation. We also reported a new ATRA-  
276 inducible component of the signalsome, Vav1. Vav1 is a guanine nucleotide exchange  
277 factor for Rho family GTPases that activate pathways leading to actin cytoskeletal re-  
278 arrangements and transcriptional alterations (30). The Vav1/Raf association correlated  
279 with Raf activity, was ATRA-inducible and decreased after treatment with the Raf inhibitor  
280 GW5074.

281 Naturally occurring cell fate decisions often incorporate reinforcing feedback and bista-  
282 bility (31, 32). One of the most well studied cell fate circuits is the Mos mitogen-activated  
283 protein kinase cascade in *Xenopus* oocytes. This cascade is activated when oocytes are  
284 induced by the steroid hormone progesterone (33). The MEK-dependent activation of

285 p42 MAPK stimulates the accumulation of the Mos oncoprotein, which in turn activates  
286 MEK, thereby closing the feedback loop. This is similar to the signal initiation module  
287 presented here; ATRA drives signalsome formation, which activates MAPK, which in turn  
288 leads to more signalsome activation. Thus, while HL-60 and *Xenopus* oocytes are vastly  
289 different biological models, their cell fate programs share a similar architectural feature.  
290 Reinforcing feedback and bistability has also been implicated in hematopoietic cell fate  
291 determination. Laslo et al showed that the counter antagonistic repressors, Gfi-1 and  
292 Egr-1/2 (whose expression is tuned by PU.1 and C/EBPa), encodes a bistable switch that  
293 results in a macrophage, neutrophil or a mixed lineage population depending upon PU.1  
294 and C/EBPa expression (32). The current model contained the Gfi-1 and Egr-1/2 agonis-  
295 tic switch; however, its significance was unclear for HL-60 cells. The expression of Gfi-1,  
296 Egr-1/2, C/EBPa and PU.1 was not consistent with the canonical lineage pattern expected  
297 from literature. For example, Egr-1/2 expression (associated with a macrophage lineage)  
298 increased, while Gfi-1 expression (associated with a neutrophil lineage) remained con-  
299 stant following ATRA exposure. Literature evidence in nonmalignant myelomonocytic fate  
300 selection has shown that Gfi-1 and Egr-1/2 promote granulocytic and monocytic differ-  
301 entiation, respectively (32). Thus, HL-60 cells, which are a less mature cancer cell line,  
302 exhibited a non-canonical expression pattern. Other unrelated cell fate decisions such  
303 as programmed cell death have also been suggested to be bistable (34). Still more bio-  
304 chemical networks important to human health, for example the human coagulation or  
305 complement cascades, also feature strong positive feedback elements (35). Thus, while  
306 reinforcing feedback is often undesirable in human engineered systems, it is at the core  
307 of a diverse variety of cell fate programs and other networks important to human health.

308 Analysis of the signal integration and phenotype modules suggested that Gfi-1 and  
309 PPAR $\gamma$  were required for ATRA-induced differentiation in HL-60 cells. Model analysis  
310 showed that PU.1, Egr-1 and C/EBPa expression increased in Gfi-1 $^{-/-}$  mutants, where

311 PU.1 expression was upregulated by greater than 8-fold. PU.1, a member of the *ets* tran-  
312 scription factor family, is a well known regulator of granulocyte and monocyte development  
313 (36). The relative level of PU.1 and C/EBPa is thought to control macrophage versus neu-  
314 trophil cell fate decisions in granulocytic macrophage progenitor cells (37). Simulations  
315 suggested that combined Gfi-1 + PPARg deletion crippled the ability of HL-60 cells to  
316 undergo neutrophilic differentiation following ATRA exposure. p21 expression decreased  
317 significantly, suggesting Gfi-1<sup>-/-</sup> + PPARg<sup>-/-</sup> mutants were less likely to G0-arrest fol-  
318 lowing ATRA exposure. The expression of other neutrophilic markers, such as CD38,  
319 also decreased in Gfi-1<sup>-/-</sup> + PPARg<sup>-/-</sup> cells. On the other hand, the expression of re-  
320 active oxygen metabolic markers, or other important transcription factors such as OCT4  
321 did not change. For example, model analysis suggested that the C/EBPa dependent in-  
322 teraction of PU.1 with the *NCF1* gene, which encodes the p47Phox protein, was the most  
323 sensitive PU.1 connection; deletion of this connection removed the ability of the system  
324 to express p47Phox. p47Phox, also known as neutrophil cytosol factor 1, is one of four  
325 cytosolic subunits of the multi-protein NADPH oxidase complex found in neutrophils (38).  
326 This enzyme is responsible for reactive oxygen species (ROS) production, a key compo-  
327 nent of the anti-microbial function of neutrophils. However, Gfi-1 deletion did not increase  
328 p47Phox expression, nor did the deletion of PPARg. This suggested that while p47Phox  
329 expression required C/EBPa and PU.1, it was saturated with respect these proteins, and  
330 simultaneously not sensitive to PPARg abundance. Together, Gfi-1<sup>-/-</sup> + PPARg<sup>-/-</sup> cells  
331 were predicted to exhibit some aspects of the ATRA response, but not other critical fea-  
332 tures such as cell cycle arrest. Hock et al showed that Gfi-1<sup>-/-</sup> mice lacked normal  
333 neutrophils, and were highly sensitive to bacterial infection (39). Thus, the model analysis  
334 was consistent with this study. However, other predictions concerning the behavior of the  
335 Gfi-1<sup>-/-</sup> + PPARg<sup>-/-</sup> mutants have yet to be verified experimentally.

336 Immunoprecipitation studies identified a limited number of ATRA-dependent and -

337 independent Raf interaction partners. While we were unable to detect the association  
338 of Raf with common kinases and GTPases such as PKC, PKA, p38, Rac and Rho, we  
339 did establish potential interactions between Raf and key partners such as Vav1, Src, Akt,  
340 CK2 and 14-3-3. All of these partners are known to be associated with Raf activation  
341 or function. Src is known to bind Raf through an SH2 domain, and this association has  
342 been shown to be dependent of the serine phosphorylation of Raf (40). Thus, an ATRA in-  
343 ducible Src/Raf association may be a result of ATRA-induced Raf phosphorylation at S259  
344 or S621. We also identified an interaction between Raf and the Ser/Thr kinases Akt and  
345 CK2. Akt can phosphorylate Raf at S259, as demonstrated by studies in a human breast  
346 cancer line (41). CK2 can also phosphorylate Raf, although the literature has traditionally  
347 focused on S338 and not S621 or S259(42). However, neither of these kinase interactions  
348 were ATRA-inducible, suggesting their association with Raf alone was not associated with  
349 ATRA-induced Raf phosphorylation. The adapter protein 14-3-3 was also constitutively  
350 associated with Raf. The interaction between Raf and 14-3-3 has been associated with  
351 both S621 and S259 phosphorylation and activity (43). Additionally, the association of  
352 Raf with 14-3-3 not only stabilized S621 phosphorylation, but also reversed the S621  
353 phosphorylation from inhibitory to activating (44). Finally, we found that Vav1/Raf associ-  
354 ation correlated with Raf activity, was ATRA-inducible and decreased after treatment with  
355 GW5074. The presence of Vav1 in Raf/Grb2 complexes has been shown to correlate with  
356 increased Raf activity in mast cells (45). Furthermore, studies on Vav1 knockout mice  
357 demonstrated that the loss of Vav1 resulted in deficiencies of ERK signaling for both T-  
358 cells as well as neutrophils (46, 47). Interestingly, while an integrin ligand-induced ROS  
359 response was blocked in Vav1 knockout neutrophils, TPA was able to bypass the Vav1  
360 requirement and stimulate both ERK phosphorylation and ROS induction (47). In this  
361 study, the TPA-induced ROS response was dependent upon Raf kinase activity, and was  
362 mitigated by the addition of GW5074. It is possible that Vav1 is downstream of various

363 integrin receptors but upstream of Raf in terms of inducible ROS responses. Vav1 has  
364 also been shown to associate with a Cbl-Slp76-CD38 complex in an ATRA-dependent  
365 manner; furthermore, transfection of HL-60 cells with Cbl mutants that fail to bind CD38,  
366 yet still bind Slp76 and Vav1, prevents ATRA-induced MAPK activation (13). The literature  
367 suggest a variety of possible receptor-signaling pathways, which involve Vav1, for MAPK  
368 activation; moreover, given the ATRA-inducible association Vav1 may play a direct role in  
369 Raf activation.

370 We hypothesized that Vav1 is a member of an ATRA-inducible complex which propels  
371 sustained MAPK activation, arrest and differentiation. Initially, ATRA-induced Vav1 ex-  
372 pression drives increased association between Vav1 and Raf. This increased interaction  
373 facilitates phosphorylation and activation of Raf by pre-bound Akt and/or CK2 at S621  
374 or perhaps S259. Constitutively bound 14-3-3 may also stabilize the S621 phosphory-  
375 lation, modulate the activity and/or up-regulate autophosphorylation. Activated Raf can  
376 then drive ERK activation, which in turn closes the positive feedback loop by activating  
377 Raf transcription factors e.g., Sp1 and/or STAT1 (48–51). We tested this working hy-  
378 pothesis using mathematical modeling. The model recapitulated both ATRA time-course  
379 data as well as the GW5074 inhibitor effects. This suggested the proposed Raf-Vav1  
380 architecture was at least consistent with the experimental studies. Further, analysis of  
381 the Raf-Vav1 model identified bistability in ppERK levels. Thus, two possible MAPK ac-  
382 tivation branches were possible for experimentally testable ATRA values. The analysis  
383 also suggested the ATRA-induced Raf-Vav1 architecture could be locked into a sustained  
384 signaling mode (high ppERK) even in the absence of a ATRA signal. This locked-in prop-  
385 erty could give rise to an ATRA-induction memory. We validated the treatment memory  
386 property predicted by the Raf-Vav1 circuit experimentally using ATRA-washout experi-  
387 ments. ERK phosphorylation levels remained high for more than 96 hr after ATRA was  
388 removed. Previous studies demonstrated that HL-60 cells possessed an inheritable mem-

389 ory of ATRA stimulus (52). Although the active state was self-sustaining, the inactive state  
390 demonstrated considerable robustness to perturbation. For example, we found that 50x  
391 overexpression of Raf was required to reliably lock MAPK into the activated state, while  
392 small perturbations had almost no effect on ppERK levels over the entire ensemble. CD38  
393 expression correlated with the ppERK, suggesting its involvement in the signaling com-  
394 plex. Our computational and experimental results showed that positive feedback, through  
395 ERK-dependent Raf expression, could sustain MAPK signaling through many division cy-  
396 cles. Such molecular mechanisms could underly aspects of cellular memory associated  
397 to consecutive ATRA treatments.

398 **Materials and Methods**

399 *Effective gene expression model equations.* We decomposed the ATRA-induced differ-  
 400 entiation program into three modules; a signal initiation module that sensed and trans-  
 401 formed the ATRA signal into activated cRaf-pS621 and the ATRA-RXR/RAR (activated  
 402 Trigger) signals; a signal integration module that controlled the expression of upstream  
 403 transcription factors given cRaf-pS621 and activated Trigger signals; and a phenotype  
 404 module which encoded the expression of functional differentiation markers from the ATRA-  
 405 inducible transcription factors. The output of the signal initiation module was the input to  
 406 the gene expression model. For each gene  $j = 1, 2, \dots, \mathcal{G}$ , we modeled both the mRNA  
 407 ( $m_j$ ), protein ( $p_j$ ) and signaling species abundance:

$$\frac{dm_j}{dt} = r_{T,j} - (\mu + \theta_{m,j}) m_j + \lambda_j \quad (1)$$

$$\frac{dp_j}{dt} = r_{X,j} - (\mu + \theta_{p,j}) p_j \quad (2)$$

$$g(p_1, \dots, p_{\mathcal{G}}, \kappa) = 0 \quad (3)$$

408 The terms  $r_{T,j}$  and  $r_{X,j}$  denote the specific rates of transcription, and translation while  
 409 the terms  $\theta_{m,j}$  and  $\theta_{p,j}$  denote first-order degradation constants for mRNA and protein,  
 410 respectively. The specific transcription rate  $r_{T,j}$  was modeled as the product of a kinetic  
 411 term  $\bar{r}_{T,j}$  and a control term  $u_j$  which described how the abundance of transcription fac-  
 412 tors, or other regulators influenced the expression of gene  $j$ . The kinetic transcription  
 413 term  $\bar{r}_{T,j}$  was modeled as:

$$\bar{r}_{T,j} = V_T^{max} \left( \frac{L_{T,o}}{L_{T,j}} \right) \left( \frac{G_j}{K_T + G_j} \right) \quad (4)$$

414 where the maximum gene expression rate  $V_T^{max}$  was defined as the product of a char-  
 415 acteristic transcription rate constant ( $k_T$ ) and the abundance of RNA polymerase ( $R_1$ ),

416  $V_T^{max} = k_T(R_1)$ . The  $(L_{T,o}/L_{T,j})$  term denotes the ratio of transcription read lengths;  $L_{T,o}$   
 417 represents a characteristic gene length, while  $L_{T,j}$  denotes the length of gene  $j$ . Thus,  
 418 the ratio  $(L_{T,o}/L_{T,j})$  is a gene specific correction to the characteristic transcription rate  
 419  $V_T^{max}$ . The degradation rate constants were defined as  $\theta_{m,j}$  and  $\theta_{p,j}$  denote characteristic  
 420 degradation constants for mRNA and protein, respectively. Lastly, the  $\lambda_j$  term denotes the  
 421 constitutive rate of expression of gene  $j$ .

422 The gene expression control term  $0 \leq u_j \leq 1$  depended upon the combination of fac-  
 423 tors which influenced the expression of gene  $j$ . If the expression of gene  $j$  was influenced  
 424 by  $1, \dots, m$  factors, we modeled this relationship as  $u_j = \mathcal{I}_j(f_{1j}(\cdot), \dots, f_{mj}(\cdot))$  where  
 425  $0 \leq f_{ij}(\cdot) \leq 1$  denotes a regulatory transfer function quantifying the influence of factor  $i$   
 426 on the expression of gene  $j$ , and  $\mathcal{I}_j(\cdot)$  denotes an integration rule which combines the  
 427 individual regulatory inputs for gene  $j$  into a single control term. In this study, the integra-  
 428 tion rule governing gene expression was the weighted fraction of promoter configurations  
 429 that resulted in gene expression (53):

$$u_j = \frac{W_{R_{1,j}} + \sum_n W_{nj} f_{nj}}{1 + W_{R_{1,j}} + \sum_d W_{dj} f_{dj}} \quad (5)$$

430 The numerator, the weighted sum (with weights  $W_{nj}$ ) of promoter configurations leading to  
 431 gene expression, was normalized by all possible promoter configurations. The likelihood  
 432 of each configuration was quantified by the transfer function  $f_{nj}$  (which we modeled using  
 433 hill like functions), while the lead term in the numerator  $W_{R_{1,j}}$  denotes the weight of con-  
 434 stitutive expression for gene  $j$ . Given this formulation, the rate of constitutive expression  
 435 was then given by:

$$\lambda_j = \bar{r}_{T,j} \left( \frac{W_{R_{1,j}}}{1 + W_{R_{1,j}}} \right) \quad (6)$$

436 If a gene expression process had no modifying factors,  $u_j = 1$ . Lastly, the specific trans-

437 lation rate was modeled as:

$$r_{X,j} = V_X^{\max} \left( \frac{L_{X,o}}{L_{X,j}} \right) \left( \frac{m_j}{K_X + m_j} \right) \quad (7)$$

438 where  $V_X^{\max}$  denotes a characteristic maximum translation rate estimated from literature,  
439 and  $K_X$  denotes a translation saturation constant. The characteristic maximum translation  
440 rate was defined as the product of a characteristic translation rate constant ( $k_X$ ) and  
441 the Ribosome abundance ( $R_2$ ),  $V_X^{\max} = k_X (R_2)$ . As was the case for transcription, we  
442 corrected the characteristic translation rate by the ratio of the length of a characteristic  
443 transcription normalized by the length of transcript  $j$ .

444 *Signaling model equations.* The signal initiation, and integration modules required the  
445 abundance of cRaf-pS621 and ATRA-RXR/RAR (activated Trigger) as inputs. However,  
446 our base model described only the abundance of inactive proteins e.g., cRaf or RXR/RAR  
447 but not the activated forms. To address this issue, we estimated pseudo steady state  
448 approximations for the abundance of cRaf-pS621 and activated Trigger (shown generally  
449 as Eq (3)). The abundance of activated trigger ( $x_{a,1}$ ) was estimated directly from the  
450 RXR/RAR abundance ( $x_{u,1}$ ):

$$x_{a,1} \sim x_{u,1} \left( \frac{\alpha \cdot \text{ATRA}}{1 + \alpha \cdot \text{ATRA}} \right) \quad (8)$$

451 where  $\alpha$  denotes a gain parameter;  $\alpha = 0.0$  if ATRA is less than a threshold, and  $\alpha = 0.1$   
452 if ATRA is greater than the differentiation threshold. The abundance of cRaf-pS621 was  
453 estimated by making the pseudo steady state approximation on the cRaf-pS621 balance.  
454 The abundance of an activated signaling species  $i$  was given by:

$$\frac{dx_i}{dt} = r_{+,i}(\mathbf{x}, \mathbf{k}) - (\mu + k_{d,i}) x_i \quad i = 1, \dots, \mathcal{M} \quad (9)$$

455 The quantity  $x_i$  denotes concentration of signaling species  $i$ , while  $\mathcal{R}$  and  $\mathcal{M}$  denote  
 456 the number of signaling reactions and signaling species in the model, respectively. The  
 457 term  $r_{+,i}(\mathbf{x}, \mathbf{k})$  denotes the rate of generation of activated species  $i$ , while  $\mu$  denotes  
 458 the specific growth rate, and  $k_{d,i}$  denotes the rate constant controlling the non-specific  
 459 degradation of  $x_i$ . We neglected deactivation reactions e.g., phosphatase activities. We  
 460 assumed that signaling processes were fast compared to gene expression; this allowed  
 461 us to approximate the signaling balance as:

$$x_i^* \simeq \frac{r_{+,i}(\mathbf{x}, \mathbf{k})}{(\mu + k_{d,i})} \quad i = 1, \dots, \mathcal{M} \quad (10)$$

462 The generation rate was written as the product of a kinetic term ( $\bar{r}_{+,i}$ ) and a control term  
 463 ( $v_i$ ). The control terms  $0 \leq v_j \leq 1$  depended upon the combination of factors which in-  
 464 fluenced rate process  $j$ . If rate  $j$  was influenced by  $1, \dots, m$  factors, we modeled this  
 465 relationship as  $v_j = \mathcal{I}_j(f_{1j}(\cdot), \dots, f_{mj}(\cdot))$  where  $0 \leq f_{ij}(\cdot) \leq 1$  denotes a regulatory  
 466 transfer function quantifying the influence of factor  $i$  on rate  $j$ . The function  $\mathcal{I}_j(\cdot)$  is an  
 467 integration rule which maps the output of regulatory transfer functions into a control vari-  
 468 able. In this study, we used  $\mathcal{I}_j \in \{\min, \max\}$  and hill transfer functions (54). If a process  
 469 had no modifying factors,  $v_j = 1$ . The kinetic rate of cRaf-pS621 generation  $\bar{r}_{+,cRaf}$  was  
 470 modeled as:

$$\bar{r}_{+,cRaf} = k_{+,cRaf} x_s \left( \frac{x_{cRaf}}{K_{+,cRaf} + x_{cRaf}} \right) \quad (11)$$

471 where  $x_s$  denotes the signalsome abundance, and  $K_{+,cRaf}$  denotes a saturation constant  
 472 governing cRaf-pS621 formation. The formation of cRaf-pS621 was regulated by only a  
 473 single factor, the abundance of MAPK inhibitor, thus  $v_{+,cRaf}$  took the form:

$$v_{+,cRaf} = \left( 1 - \frac{I}{K_D + I} \right) \quad (12)$$

474 where  $I$  denotes the abundance of the MAPK inhibitor, and  $K_D$  denotes the inhibitor  
475 affinity.

476 *Estimation of gene expression model parameters.* We estimated parameters appearing  
477 in the mRNA and protein balances, the abundance of polymerases and ribosomes, tran-  
478 scription and translation rates, the half-life of a typical mRNA and protein, and typical  
479 values for the copies per cell of RNA polymerase and ribosomes from literature (Table 2).  
480 The saturation constants  $K_X$  and  $K_T$  were adjusted so that gene expression and trans-  
481 lation resulted in gene products on a biologically realistic concentration scale. Lastly, we  
482 calculated the concentration for gene  $G_j$  by assuming, on average, that a cell had two  
483 copies of each gene at any given time. Thus, the bulk of our gene expression model pa-  
484 rameters were based directly upon literature values, and were not adjusted during model  
485 identification. However, the remaining parameters, e.g., the  $W_{ij}$  appearing in the gene  
486 expression control laws, or parameters appearing in the transfer functions  $f_{dij}$ , were esti-  
487 mated from the protein expression and signaling data sets discussed here.

488 Signaling and gene expression model parameters were estimated by minimizing the  
489 squared difference between simulations and experimental protein data set  $j$ . We mea-  
490 sured the squared difference in the scale, fold change and shape for protein  $j$ :

$$E_j(\mathbf{k}) = \left( \mathcal{M}_j(t_-) - \hat{y}_j(t_-, \mathbf{k}) \right)^2 + \sum_{i=1}^{\mathcal{T}_j} \left( \hat{\mathcal{M}}_{ij} - \hat{y}_{ij}(\mathbf{k}) \right)^2 + \sum_{i=1}^{\mathcal{T}_j} \left( \mathcal{M}'_{ij} - y'_{ij}(\mathbf{k}) \right)^2 \quad (13)$$

491 The first term in Eqn. (13) quantified the initial *scale* error, directly before the addition  
492 of ATRA. In this case,  $\mathcal{M}_j(t_-)$  (the approximate concentration of protein  $j$  before the  
493 addition of ATRA) was estimated from literature. This term was required because the  
494 protein measurements were reported as the fold-change; thus, the data was normalized  
495 by a control value measured before the addition of ATRA. However, the model operated on  
496 a physical scale. The first term allowed the model to capture physically realistic changes

497 following ATRA addition. The second term quantified the difference in the *fold-change* of  
 498 protein  $j$  as a function of time. The terms  $\hat{\mathcal{M}}_{ij}$  and  $\hat{y}_{ij}$  denote the scaled experimental  
 499 observations and simulation outputs (fold-change; protein normalized by control value  
 500 directly before ATRA addition) at time  $i$  from protein  $j$ , where  $T_j$  denoted the number of  
 501 time points for data set  $j$ . Lastly, the third term of the objective function measured the  
 502 difference in the *shape* of the measured and simulated protein levels. The scaled value  
 503  $0 \leq \mathcal{M}'_{ij} \leq 1$  was given by:

$$\hat{\mathcal{M}}_{ij} = \left( \mathcal{M}_{ij} - \min_i \mathcal{M}_{ij} \right) / \left( \max_i \mathcal{M}_{ij} - \min_i \mathcal{M}_{ij} \right) \quad (14)$$

504 where  $\mathcal{M}'_{ij} = 0$  and  $\mathcal{M}'_{ij} = 1$  describe the lowest (highest) intensity bands. A similar  
 505 scaling was used for the simulation output. We minimized the total model residual  $\sum_j E_j$   
 506 using a heuristic direct-search optimization procedure, subject to box constraints on the  
 507 parameter values, starting from a random initial parameter guess. Each downhill step was  
 508 archived and used for ensemble calculations. The optimization procedure (a covariance  
 509 matrix adaptation evolution strategy) has been reported previously (55).

510 *Estimation of an effective cell cycle arrest model.* We formulated an effective N-order  
 511 polynomial model of the fraction of cells undergoing ATRA-induced cell cycle arrest at  
 512 time  $t$ ,  $\hat{\mathcal{A}}(t)$ , as:

$$\hat{\mathcal{A}}(t) \simeq a_0 + \sum_{i=1}^{N-1} a_i \phi_i(\mathbf{p}(t), t) \quad (15)$$

513 where  $a_i$  were unknown parameters, and  $\phi_i(\mathbf{p}(t), t)$  denotes a basis function. The basis  
 514 functions were dependent upon the system state; in this study, we assumed  $N = 4$  and  
 515 basis functions of the form:

$$\phi_i(\mathbf{p}(t), t) = \left( \frac{t}{T} + \frac{p21}{E2F} \Big|_t \right)^{(i-1)} \quad (16)$$

516 The parameters  $a_0, \dots, a_3$  were estimated directly from cell-cycle measurements (biologi-  
517 cal replicates) using least-squares.

518 *Availability of model code.* The signaling and gene expression model equations, and the  
519 parameter estimation procedure, were implemented in the Julia programming language.  
520 The model equations were solved using the ODE23s routine of the ODE package (56). The  
521 model code and parameter ensemble is freely available under an MIT software license  
522 and can be downloaded from <http://www.varnerlab.org>.

523 *Cell culture and treatment* Human myeloblastic leukemia cells (HL-60 cells) were grown  
524 in a humidified atmosphere of 5% CO<sub>2</sub> at 37°C and maintained in RPMI 1640 from Gibco  
525 (Carlsbad, CA) supplemented with 5% heat inactivated fetal bovine serum from Hyclone  
526 (Logan, UT) and 1× antibiotic/antimicotic (Gibco, Carlsbad, CA). Cells were cultured in  
527 constant exponential growth (57). Experimental cultures were initiated at  $0.1 \times 10^6$  cells/mL  
528 24 hr prior to ATRA treatment; if indicated, cells were also treated with GW5074 (2 $\mu$ M) 18  
529 hr before ATRA treatment. For the cell culture washout experiments, cells were treated  
530 with ATRA for 24 hr, washed 3x with prewarmed serum supplemented culture medium  
531 to remove ATRA, and reseeded in ATRA-free media as described. Western blot analysis  
532 was performed at incremental time points after removal of ATRA.

533 *Chemicals* All-Trans Retinoic Acid (ATRA) from Sigma-Aldrich (St. Louis, MO) was dis-  
534 solved in 100% ethanol with a stock concentration of 5mM, and used at a final concen-  
535 tration of 1 $\mu$ M (unless otherwise noted). The cRaf inhibitor GW5074 from Sigma-Aldrich  
536 (St. Louis, MO) was dissolved in DMSO with a stock concentration of 10mM, and used  
537 at a final concentration of 2 $\mu$ M. HL-60 cells were treated with 2 $\mu$ M GW5074 with or with-  
538 out ATRA (1 $\mu$ M) at 0 hr. This GW5074 dosage had a negligible effect on the cell cycle  
539 distribution, compared to ATRA treatment alone.

540 *Immunoprecipitation and western blotting* Approximately  $1.2 \times 10^7$  cells were lysed using  
541  $400\mu\text{L}$  of M-Per lysis buffer from Thermo Scientific (Waltham, MA). Lysates were cleared  
542 by centrifugation at  $16,950 \times g$  in a micro-centrifuge for 20 min at  $4^\circ\text{C}$ . Lysates were  
543 pre-cleared using  $100\mu\text{L}$  protein A/G Plus agarose beads from Santa Cruz Biotechnology  
544 (Santa Cruz, CA) by inverting overnight at  $4^\circ\text{C}$ . Beads were cleared by centrifugation and  
545 total protein concentration was determined by a BCA assay (Thermo Scientific, Waltham,  
546 MA). Immunoprecipitations were setup by bringing lysate to a concentration of 1g/L in a  
547 total volume of  $300\mu\text{L}$  (M-Per buffer was used for dilution). The anti-Raf antibody was  
548 added at  $3\mu\text{L}$ . A negative control with no bait protein was also used to exclude the di-  
549 rect interaction of proteins with the A/G beads. After 1 hr of inversion at  $4^\circ\text{C}$ ,  $20\mu\text{L}$  of  
550 agarose beads was added and samples were left to invert overnight at  $4^\circ\text{C}$ . Samples  
551 were then washed three times with M-Per buffer by centrifugation. Finally proteins were  
552 eluted from agarose beads using a laemmli loading buffer. Eluted proteins were resolved  
553 by SDS-PAGE and Western blotting. Total lysate samples were normalized by total protein  
554 concentration ( $20\mu\text{g}$  per sample) and resolved by SDS-PAGE and Western blotting. Sec-  
555 ondary HRP bound antibody was used for visualization. All antibodies were purchased  
556 from Cell Signaling (Boston, MA) with the exception of  $\alpha$ -p621 Raf which was purchased  
557 from Biosource/Invitrogen (Carlsbad, CA), and  $\alpha$ -CK2 from BD Biosciences (San Jose,  
558 CA).

559 *Morphology assessment* Untreated and ATRA-treated HL-60 cells were collected after  
560 72 hr and cytocentrifuged for 3 min at 700 rpm onto glass slides. Slides were air-dried  
561 and stained with Wright's stain. Slide images were captured at 40X (Leica DM LB 100T  
562 microscope, Leica Microsystems).

563 **Competing interests**

564 The authors declare that they have no competing interests.

565 **Author's contributions**

566 J.V and A.Y directed the study. R.T, H.J, R.B and J.C conducted the cell culture measure-  
567 ments. J.V, R.B, W.D, K.R and A.S developed the reduced order HL-60 models and the  
568 parameter ensemble. W.D and J.V analyzed the model ensemble, and generated figures  
569 for the manuscript. The manuscript was prepared and edited for publication by W.D, A.Y  
570 and J.V.

571 **Acknowledgements**

572 We gratefully acknowledge the suggestions from the anonymous reviewers to improve  
573 this manuscript.

574 **Funding**

575 We acknowledge the financial support to J.V. by the National Science Foundation CA-  
576 REER (CBET-0846876) for the support of R.T. and H.J. In addition, we acknowledge  
577 support to A.Y. from the National Institutes of Health (CA 30555, CA152870) and a grant  
578 from New York State Stem Cell Science. Lastly, we acknowledge the financial support to  
579 J.V. and A.Y. from the National Cancer Institute (#U54 CA143876). The content is solely  
580 the responsibility of the authors and does not necessarily represent the official views of  
581 the National Cancer Institute or the National Institutes of Health.

582 **References**

- 583 1. Bushue N, Wan YJY (2010) Retinoid pathway and cancer therapeutics. *Adv Drug  
584 Deliv Rev* 62: 1285-98.
- 585 2. Tang XH, Gudas LJ (2011) Retinoids, retinoic acid receptors, and cancer. *Annu Rev  
586 Pathol* 6: 345-64.
- 587 3. Cheung FSG, Lovicu FJ, Reichardt JKV (2012) Current progress in using vitamin d  
588 and its analogs for cancer prevention and treatment. *Expert Rev Anticancer Ther*  
589 12: 811-37.
- 590 4. Nilsson B (1984) Probable in vivo induction of differentiation by retinoic acid of  
591 promyelocytes in acute promyelocytic leukaemia. *Br J Haematol* 57: 365-71.
- 592 5. Warrell RP Jr (1993) Retinoid resistance in acute promyelocytic leukemia: new  
593 mechanisms, strategies, and implications. *Blood* 82: 1949-53.
- 594 6. Freemantle SJ, Spinella MJ, Dmitrovsky E (2003) Retinoids in cancer therapy and  
595 chemoprevention: promise meets resistance. *Oncogene* 22: 7305-15.
- 596 7. Breitman TR, Selonick SE, Collins SJ (1980) Induction of differentiation of the hu-  
597 man promyelocytic leukemia cell line (HL-60) by retinoic acid. *Proc Natl Acad Sci U  
598 S A* 77: 2936–2940.
- 599 8. Yen A, Roberson MS, Varvayanis S, Lee AT (1998) Retinoic acid induced  
600 mitogen-activated protein (MAP)/extracellular signal-regulated kinase (ERK) kinase-  
601 dependent MAP kinase activation needed to elicit HL-60 cell differentiation and  
602 growth arrest. *Cancer Res* 58: 3163–3172.
- 603 9. Hong HY, Varvayanis S, Yen A (2001) Retinoic acid causes MEK-dependent RAF  
604 phosphorylation through RARalpha plus RXR activation in HL-60 cells. *Differentia-  
605 tion* 68: 55–66.
- 606 10. Mangelsdorf DJ, Ong ES, Dyck JA, Evans RM (1990) Nuclear receptor that identifies  
607 a novel retinoic acid response pathway. *Nature* 345: 224–229.

- 608 11. Congleton J, MacDonald R, Yen A (2012) Src inhibitors, PP2 and dasatinib, increase  
609 retinoic acid-induced association of Lyn and c-Raf (S259) and enhance MAPK-  
610 dependent differentiation of myeloid leukemia cells. Leukemia 26: 1180-8.
- 611 12. Shen M, Bunaci R, Congleton J, Jensen H, Sayam L, et al. (2011) Interferon regu-  
612 latory factor-1 binds c-Cbl, enhances mitogen activated protein kinase signaling and  
613 promotes retinoic acid-induced differentiation of HL-60 human myelo-monoblastic  
614 leukemia cells. Leuk Lymphoma 52: 2372-9.
- 615 13. Shen M, Yen A (2009) c-Cbl tyrosine kinase-binding domain mutant G306E abol-  
616 ishes the interaction of c-Cbl with CD38 and fails to promote retinoic acid-induced  
617 cell differentiation and G0 arrest. J Biol Chem 284: 25664–25677.
- 618 14. Yen A, Varvayanis S, Smith J, Lamkin T (2006) Retinoic acid induces expression of  
619 SLP-76: expression with c-FMS enhances ERK activation and retinoic acid-induced  
620 differentiation/G0 arrest of HL-60 cells. Eur J Cell Biol 85: 117–132.
- 621 15. Marchisio M, Bertagnolo V, Colamussi ML, Capitani S, Neri LM (1998) Phos-  
622 phatidylinositol 3-kinase in HL-60 nuclei is bound to the nuclear matrix and increases  
623 during granulocytic differentiation. Biochem Biophys Res Commun 253: 346-51.
- 624 16. Congleton J, Jiang H, Malavasi F, Lin H, Yen A (2011) ATRA-induced HL-60 myeloid  
625 leukemia cell differentiation depends on the CD38 cytosolic tail needed for mem-  
626 brane localization, but CD38 enzymatic activity is unnecessary. Exp Cell Res 317:  
627 910–919.
- 628 17. Wang J, Yen A (2004) A novel retinoic acid-responsive element regulates retinoic  
629 acid induced BLR1 expression. Mol Cell Biol 24: 2423 - 2443.
- 630 18. Yen A (1990) HL-60 cells as a model of growth and differentiation: the significance  
631 of variant cells. Hematology Review 4: 5-46.
- 632 19. Yang T, Xiong Q, Enslen H, Davis R, Chow CW (2002) Phosphorylation of NFATc4  
633 by p38 mitogen-activated protein kinases. Mol Cell Biol 22: 3892–3904.

- 634 20. Wang J, Yen A (2008) A MAPK-positive Feedback Mechanism for BLR1 Signaling  
635 Propels Retinoic Acid-triggered Differentiation and Cell Cycle Arrest. *J Biol Chem*  
636 283: 4375–4386.
- 637 21. Tasseff R, Nayak S, Song S, Yen A, Varner J (2011) Modeling and analysis of retinoic  
638 acid induced differentiation of uncommitted precursor cells. *Integr Biol* 3: 578 - 591.
- 639 22. Jensen HA, Styskal LE, Tasseff R, Bunaciu RP, Congleton J, et al. (2013) The  
640 src-family kinase inhibitor pp2 rescues inducible differentiation events in emergent  
641 retinoic acid-resistant myeloblastic leukemia cells. *PLoS One* 8: e58621.
- 642 23. Jensen HA, Bunaciu RP, Ibabao CN, Myers R, Varner JD, et al. (2014) Retinoic acid  
643 therapy resistance progresses from unilineage to bilineage in hl-60 leukemic blasts.  
644 *PLoS One* 9: e98929.
- 645 24. Jensen HA, Bunaciu RP, Varner JD, Yen A (2015) Gw5074 and pp2 kinase inhibitors  
646 implicate nontraditional c-raf and lyn function as drivers of retinoic acid-induced mat-  
647 uration. *Cell Signal* 27: 1666-75.
- 648 25. Jensen HA, Yourish HB, Bunaciu RP, Varner JD, Yen A (2015) Induced myelomono-  
649 cytic differentiation in leukemia cells is accompanied by noncanonical transcription  
650 factor expression. *FEBS Open Bio* 5: 789-800.
- 651 26. Milo R, Jorgensen P, Moran U, Weber G, Springer M (2010) Bionumbers—the  
652 database of key numbers in molecular and cell biology. *Nucleic Acids Res* 38: D750-  
653 3.
- 654 27. Katagiri K, Hattori S, Nakamura S, Yamamoto T, Yoshida T, et al. (1994) Activation  
655 of ras and formation of gap complex during tpa-induced monocytic differentiation of  
656 hl-60 cells. *Blood* 84: 1780–1789.
- 657 28. Miranda MB, Johnson DE (2007) Signal transduction pathways that contribute to  
658 myeloid differentiation. *Leukemia* 21: 1363–1377.
- 659 29. Hickstein DD, Back AL, Collins SJ (1989) Regulation of expression of the cd11b and

- 660 cd18 subunits of the neutrophil adherence receptor during human myeloid differen-  
661 tiation. *J Biol Chem* 264: 21812–21817.
- 662 30. Hornstein I, Alcover A, Katzav S (2004) Vav proteins, masters of the world of cy-  
663 toskeleton organization. *Cell Signal* 16: 1-11.
- 664 31. Ferrell J (2002) Self-perpetuating states in signal transduction: positive feedback,  
665 double-negative feedback and bistability. *Curr Opin Cell Biol* 14: 140-8.
- 666 32. Laslo P, Spooner CJ, Warmflash A, Lancki DW, Lee HJ, et al. (2006) Multilineage  
667 transcriptional priming and determination of alternate hematopoietic cell fates. *Cell*  
668 126: 755-66.
- 669 33. Xiong W, Ferrell J (2003) A positive-feedback-based bistable 'memory module' that  
670 governs a cell fate decision. *Nature* 426: 460-5.
- 671 34. Bagci EZ, Vodovotz Y, Billiar TR, Ermentrout GB, Bahar I (2006) Bistability in apop-  
672 tosis: roles of bax, bcl-2, and mitochondrial permeability transition pores. *Biophys J*  
673 90: 1546-59.
- 674 35. Luan D, Zai M, Varner JD (2007) Computationally derived points of fragility of a  
675 human cascade are consistent with current therapeutic strategies. *PLoS Comput  
676 Biol* 3: e142.
- 677 36. Friedman AD (2007) Transcriptional control of granulocyte and monocyte develop-  
678 ment. *Oncogene* 26: 6816-28.
- 679 37. Dahl R, Walsh JC, Lancki D, Laslo P, Iyer SR, et al. (2003) Regulation of macrophage  
680 and neutrophil cell fates by the PU.1:C/EBPalpha ratio and granulocyte colony-  
681 stimulating factor. *Nat Immunol* 4: 1029-36.
- 682 38. El-Benna J, Dang PMC, Gougerot-Pocidalo MA, Marie JC, Braut-Boucher F (2009)  
683 p47phox, the phagocyte nadph oxidase/nox2 organizer: structure, phosphorylation  
684 and implication in diseases. *Exp Mol Med* 41: 217-25.
- 685 39. Hock H, Hamblen MJ, Rooke HM, Traver D, Bronson RT, et al. (2003) Intrinsic re-

- 686 requirement for zinc finger transcription factor gfi-1 in neutrophil differentiation. Immuno-  
687 nity 18: 109-20.
- 688 40. Cleghon V, Morrison DK (1994) Raf-1 interacts with fyn and src in a non-  
689 phosphotyrosine-dependent manner. J Biol Chem 269: 17749–17755.
- 690 41. Zimmermann S, Moelling K (1999) Phosphorylation and regulation of raf by akt (pro-  
691 tein kinase b). Science 286: 1741–1744.
- 692 42. Ritt DA, Zhou M, Conrads TP, Veenstra TD, Copeland TD, et al. (2007) Ck2 is a  
693 component of the ksr1 scaffold complex that contributes to raf kinase activation.  
694 Curr Biol 17: 179–184.
- 695 43. Hekman M, Wiese S, Metz R, Albert S, Troppmair J, et al. (2004) Dynamic changes  
696 in c-raf phosphorylation and 14-3-3 protein binding in response to growth factor stim-  
697 ulation: differential roles of 14-3-3 protein binding sites. J Biol Chem 279: 14074–  
698 14086.
- 699 44. Dhillon AS, Yip YY, Grindlay GJ, Pakay JL, Dangers M, et al. (2009) The c-terminus  
700 of raf-1 acts as a 14-3-3-dependent activation switch. Cell Signal 21: 1645–1651.
- 701 45. Song JS, Gomez J, Stancato LF, Rivera J (1996) Association of a p95 vav-containing  
702 signaling complex with the fcepsiloniori gamma chain in the rbl-2h3 mast cell line.  
703 evidence for a constitutive in vivo association of vav with grb2, raf-1, and erk2 in an  
704 active complex. J Biol Chem 271: 26962–26970.
- 705 46. Costello PS, Walters AE, Mee PJ, Turner M, Reynolds LF, et al. (1999) The rho-  
706 family gtp exchange factor vav is a critical transducer of t cell receptor signals to the  
707 calcium, erk, and nf-kappab pathways. Proc Natl Acad Sci U S A 96: 3035–3040.
- 708 47. Graham D, Robertson C, Bautista J, Mascarenhas F, Diacovo M, et al. (2007)  
709 Neutrophil-mediated oxidative burst and host defense are controlled by a Vav-  
710 PLCgamma2 signaling axis in mice. J Clin Invest 117: 3445–3452.
- 711 48. Kim HS, Lim IK (2009) Phosphorylated extracellular signal-regulated protein kinases

- 712 1 and 2 phosphorylate sp1 on serine 59 and regulate cellular senescence via tran-  
713 scription of p21sdi1/cip1/waf1. *J Biol Chem* 284: 15475–15486.
- 714 49. Milanini-Mongiat J, Pouyss?gur J, Pag?s G (2002) Identification of two sp1 phos-  
715 phorylation sites for p42/p44 mitogen-activated protein kinases: their implication in  
716 vascular endothelial growth factor gene transcription. *J Biol Chem* 277: 20631–  
717 20639.
- 718 50. Zhang Y, Cho YY, Petersen BL, Zhu F, Dong Z (2004) Evidence of stat1 phosphor-  
719 ylation modulated by mapks, mek1 and msk1. *Carcinogenesis* 25: 1165–1175.
- 720 51. Li Z, Theus MH, Wei L (2006) Role of erk 1/2 signaling in neuronal differentiation of  
721 cultured embryonic stem cells. *Dev Growth Differ* 48: 513–523.
- 722 52. Yen A, Reece SL, Albright KL (1984) Dependence of hl-60 myeloid cell differentiation  
723 on continuous and split retinoic acid exposures: precommitment memory associated  
724 with altered nuclear structure. *J Cell Physiol* 118: 277–286.
- 725 53. Moon TS, Lou C, Tamsir A, Stanton BC, Voigt CA (2012) Genetic programs con-  
726 structed from layered logic gates in single cells. *Nature* 491: 249-53.
- 727 54. Wayman JA, Sagar A, Varner JD (2015) Dynamic modeling of cell-free biochemical  
728 networks using effective kinetic models. *Processes* 3: 138.
- 729 55. Igel C, Hansen N, Roth S (2007) Covariance matrix adaptation for multi-objective  
730 optimization. *Evol Comput* 15: 1-28.
- 731 56. Bezanson J, Edelman A, Karpinski S, Shah VB (2014) Julia: A fresh approach to  
732 numerical computing. *CoRR* abs/1411.1607.
- 733 57. Brooks SC, Kazmer S, Levin AA, Yen A (1996) Myeloid differentiation and retinoblas-  
734 toma phosphorylation changes in HL-60 cells induced by retinoic acid receptor- and  
735 retinoid X receptor-selective retinoic acid analogs. *Blood* 87: 227–237.
- 736 58. Rishi AK, Gerald TM, Shao ZM, Li XS, Baumann RG, et al. (1996) Regulation of the  
737 human retinoic acid receptor alpha gene in the estrogen receptor negative human

- 738 breast carcinoma cell lines skbr-3 and mda-mb-435. Cancer Res 56: 5246-52.

739 59. Mueller BU, Pabst T, Fos J, Petkovic V, Fey MF, et al. (2006) Atra resolves the dif-  
740 ferentiation block in t(15;17) acute myeloid leukemia by restoring pu.1 expression.  
741 Blood 107: 3330-8.

742 60. Luo XM, Ross AC (2006) Retinoic acid exerts dual regulatory actions on the ex-  
743 pression and nuclear localization of interferon regulatory factor-1. Exp Biol Med  
744 (Maywood) 231: 619-31.

745 61. Sylvester I, Schöler HR (1994) Regulation of the oct-4 gene by nuclear receptors.  
746 Nucleic Acids Res 22: 901-11.

747 62. Drach J, McQueen T, Engel H, Andreeff M, Robertson KA, et al. (1994) Retinoic  
748 acid-induced expression of cd38 antigen in myeloid cells is mediated through  
749 retinoic acid receptor-alpha. Cancer Res 54: 1746-52.

750 63. Liu M, Iavarone A, Freedman LP (1996) Transcriptional activation of the human  
751 p21(waf1/cip1) gene by retinoic acid receptor. correlation with retinoid induction of  
752 u937 cell differentiation. J Biol Chem 271: 31723-8.

753 64. Bunaciu RP, Yen A (2013) 6-formylindolo (3,2-b)carbazole (ficz) enhances retinoic  
754 acid (ra)-induced differentiation of hl-60 myeloblastic leukemia cells. Mol Cancer 12:  
755 39.

756 65. Balmer JE, Blomhoff R (2002) Gene expression regulation by retinoic acid. J Lipid  
757 Res 43: 1773-808.

758 66. Rosen ED, Hsu CH, Wang X, Sakai S, Freeman MW, et al. (2002) C/ebpalpha in-  
759 duces adipogenesis through ppargamma: a unified pathway. Genes Dev 16: 22-6.

760 67. Varley CL, Bacon EJ, Holder JC, Southgate J (2009) Foxa1 and irf-1 intermediary  
761 transcriptional regulators of ppargamma-induced urothelial cytodifferentiation. Cell  
762 Death Differ 16: 103-14.

763 68. Bruemmer D, Yin F, Liu J, Berger JP, Sakai T, et al. (2003) Regulation of the growth

- 764 arrest and dna damage-inducible gene 45 (gadd45) by peroxisome proliferator-  
765 activated receptor gamma in vascular smooth muscle cells. Circ Res 93: e38-47.
- 766 69. Delerive P, De Bosscher K, Besnard S, Vanden Berghe W, Peters JM, et al. (1999)  
767 Peroxisome proliferator-activated receptor alpha negatively regulates the vascular  
768 inflammatory gene response by negative cross-talk with transcription factors nf-  
769 kappaB and ap-1. J Biol Chem 274: 32048-54.
- 770 70. Altiok S, Xu M, Spiegelman BM (1997) Ppargamma induces cell cycle withdrawal:  
771 inhibition of e2f/dp dna-binding activity via down-regulation of pp2a. Genes Dev 11:  
772 1987-98.
- 773 71. Fei J, Cook C, Gillespie M, Yu B, Fullen K, et al. (2011) Atherogenic  $\omega$ -6 lipids mod-  
774 ulate ppar- egr-1 crosstalk in vascular cells. PPAR Res 2011: 753917.
- 775 72. Song EK, Lee YR, Kim YR, Yeom JH, Yoo CH, et al. (2012) Naadp mediates insulin-  
776 stimulated glucose uptake and insulin sensitization by ppar $\gamma$  in adipocytes. Cell Rep  
777 2: 1607-19.
- 778 73. Szanto A, Nagy L (2005) Retinoids potentiate peroxisome proliferator-activated re-  
779 ceptor gamma action in differentiation, gene expression, and lipid metabolic pro-  
780 cesses in developing myeloid cells. Mol Pharmacol 67: 1935-43.
- 781 74. Han S, Sidell N, Fisher PB, Roman J (2004) Up-regulation of p21 gene expres-  
782 sion by peroxisome proliferator-activated receptor gamma in human lung carcinoma  
783 cells. Clin Cancer Res 10: 1911-9.
- 784 75. Von Knethen A, Brüne B (2002) Activation of peroxisome proliferator-activated re-  
785 ceptor gamma by nitric oxide in monocytes/macrophages down-regulates p47phox  
786 and attenuates the respiratory burst. J Immunol 169: 2619-26.
- 787 76. Dispirito JR, Fang B, Wang F, Lazar MA (2013) Pruning of the adipocyte peroxisome  
788 proliferator-activated receptor  $\gamma$  cistrome by hematopoietic master regulator pu.1.  
789 Mol Cell Biol 33: 3354-64.

- 790 77. Chen H, Ray-Gallet D, Zhang P, Hetherington CJ, Gonzalez DA, et al. (1995) Pu.1  
791 (spi-1) autoregulates its expression in myeloid cells. *Oncogene* 11: 1549-60.
- 792 78. Steidl U, Rosenbauer F, Verhaak RGW, Gu X, Ebralidze A, et al. (2006) Essential  
793 role of jun family transcription factors in pu.1 knockdown-induced leukemic stem  
794 cells. *Nat Genet* 38: 1269-77.
- 795 79. Pahl HL, Scheibe RJ, Zhang DE, Chen HM, Galson DL, et al. (1993) The proto-  
796 oncogene pu.1 regulates expression of the myeloid-specific cd11b promoter. *J Biol  
797 Chem* 268: 5014-20.
- 798 80. Yuki H, Ueno S, Tatetsu H, Niiro H, Iino T, et al. (2013) Pu.1 is a potent tumor  
799 suppressor in classical hodgkin lymphoma cells. *Blood* 121: 962-70.
- 800 81. Li SL, Schlegel W, Valente AJ, Clark RA (1999) Critical flanking sequences of pu.1  
801 binding sites in myeloid-specific promoters. *J Biol Chem* 274: 32453-60.
- 802 82. Timchenko N, Wilson DR, Taylor LR, Abdelsayed S, Wilde M, et al. (1995) Autoreg-  
803 ulation of the human c/ebp alpha gene by stimulation of upstream stimulatory factor  
804 binding. *Mol Cell Biol* 15: 1192-202.
- 805 83. Lidonnici MR, Audia A, Soliera AR, Prisco M, Ferrari-Amorotti G, et al. (2010) Ex-  
806 pression of the transcriptional repressor gfi-1 is regulated by c/ebpalpha and is  
807 involved in its proliferation and colony formation-inhibitory effects in p210bcr/abl-  
808 expressing cells. *Cancer Res* 70: 7949-59.
- 809 84. D'Alo' F, Johansen LM, Nelson EA, Radomska HS, Evans EK, et al. (2003) The  
810 amino terminal and e2f interaction domains are critical for c/ebp alpha-mediated  
811 induction of granulopoietic development of hematopoietic cells. *Blood* 102: 3163-  
812 71.
- 813 85. Pan Z, Hetherington CJ, Zhang DE (1999) Ccaat/enhancer-binding protein activates  
814 the cd14 promoter and mediates transforming growth factor beta signaling in mono-  
815 cyte development. *J Biol Chem* 274: 23242-8.

- 816 86. Harris TE, Albrecht JH, Nakanishi M, Darlington GJ (2001) Ccaat/enhancer-binding  
817 protein-alpha cooperates with p21 to inhibit cyclin-dependent kinase-2 activity and  
818 induces growth arrest independent of dna binding. *J Biol Chem* 276: 29200-9.
- 819 87. Bauvois B, Durant L, Laboureau J, Barthélémy E, Rouillard D, et al. (1999) Upreg-  
820 ulation of cd38 gene expression in leukemic b cells by interferon types i and ii. *J*  
821 *Interferon Cytokine Res* 19: 1059-66.
- 822 88. Passioura T, Dolnikov A, Shen S, Symonds G (2005) N-ras-induced growth suppres-  
823 sion of myeloid cells is mediated by irf-1. *Cancer Res* 65: 797-804.
- 824 89. Dahl R, Iyer SR, Owens KS, Cuylear DD, Simon MC (2007) The transcriptional  
825 repressor gfi-1 antagonizes pu.1 activity through protein-protein interaction. *J Biol*  
826 *Chem* 282: 6473-83.
- 827 90. Duan Z, Horwitz M (2003) Targets of the transcriptional repressor oncoprotein gfi-1.  
828 *Proc Natl Acad Sci U S A* 100: 5932-7.
- 829 91. Chen H, Zhang P, Radomska HS, Hetherington CJ, Zhang DE, et al. (1996) Octamer  
830 binding factors and their coactivator can activate the murine pu.1 (spi-1) promoter.  
831 *J Biol Chem* 271: 15743-52.
- 832 92. Behre G, Whitmarsh AJ, Coghlan MP, Hoang T, Carpenter CL, et al. (1999) c-jun  
833 is a jnk-independent coactivator of the pu.1 transcription factor. *J Biol Chem* 274:  
834 4939-46.
- 835 93. Kardassis D, Papakosta P, Pardali K, Moustakas A (1999) c-jun transactivates the  
836 promoter of the human p21(waf1/cip1) gene by acting as a superactivator of the  
837 ubiquitous transcription factor sp1. *J Biol Chem* 274: 29572-81.
- 838 94. Johnson DG, Ohtani K, Nevins JR (1994) Autoregulatory control of e2f1 expression  
839 in response to positive and negative regulators of cell cycle progression. *Genes Dev*  
840 8: 1514-25.
- 841 95. Fu M, Zhang J, Lin Y, Zhu X, Ehrengruber MU, et al. (2002) Early growth response

- 842 factor-1 is a critical transcriptional mediator of peroxisome proliferator-activated  
843 receptor-gamma 1 gene expression in human aortic smooth muscle cells. J Biol  
844 Chem 277: 26808-14.
- 845 96. Mak KS, Funnell APW, Pearson RCM, Crossley M (2011) Pu.1 and haematopoietic  
846 cell fate: Dosage matters. Int J Cell Biol 2011: 808524.
- 847 97. Chen F, Wang Q, Wang X, Studzinski GP (2004) Up-regulation of egr1 by 1,25-  
848 dihydroxyvitamin d3 contributes to increased expression of p35 activator of cyclin-  
849 dependent kinase 5 and consequent onset of the terminal phase of hl60 cell differ-  
850 entiation. Cancer Res 64: 5425-33.
- 851 98. Suh J, Jeon YJ, Kim HM, Kang JS, Kaminski NE, et al. (2002) Aryl hydrocarbon  
852 receptor-dependent inhibition of ap-1 activity by 2,3,7,8-tetrachlorodibenzo-p-dioxin  
853 in activated b cells. Toxicol Appl Pharmacol 181: 116-23.
- 854 99. Shen M, Bunaciu RP, Congleton J, Jensen HA, Sayam LG, et al. (2011) Inter-  
855 feron regulatory factor-1 binds c-cbl, enhances mitogen activated protein kinase  
856 signaling and promotes retinoic acid-induced differentiation of hl-60 human myelo-  
857 monoblastic leukemia cells. Leuk Lymphoma 52: 2372-9.
- 858 100. Bunaciu RP, Yen A (2011) Activation of the aryl hydrocarbon receptor ahr promotes  
859 retinoic acid-induced differentiation of myeloblastic leukemia cells by restricting ex-  
860 pression of the stem cell transcription factor oct4. Cancer Res 71: 2371-80.
- 861 101. Jackson DA, Pombo A, Iborra F (2000) The balance sheet for transcription: an anal-  
862 ysis of nuclear rna metabolism in mammalian cells. FASEB J 14: 242-54.
- 863 102. Zhao ZW, Roy R, Gebhardt JCM, Suter DM, Chapman AR, et al. (2014) Spatial orga-  
864 nization of rna polymerase ii inside a mammalian cell nucleus revealed by reflected  
865 light-sheet superresolution microscopy. Proc Natl Acad Sci U S A 111: 681-6.
- 866 103. Freitas R, Merkle R (2004) Kinematic Self-Replicating Machines. Oxford University  
867 Press.

- 868 104. Yang E, van Nimwegen E, Zavolan M, Rajewsky N, Schroeder M, et al. (2003) Decay rates of human mRNAs: correlation with functional characteristics and sequence  
869 attributes. *Genome Res* 13: 1863-72.
- 870
- 871 105. Doherty MK, Hammond DE, Clague MJ, Gaskell SJ, Beynon RJ (2009) Turnover  
872 of the human proteome: determination of protein intracellular stability by dynamic  
873 SILAC. *J Proteome Res* 8: 104-12.
- 874
- 875 106. Sehgal PB, Derman E, Molloy GR, Tamm I, Darnell JE (1976) 5,6-dichloro-1-beta-D-ribofuranosylbenzimidazole inhibits initiation of nuclear heterogeneous RNA chains  
876 in HeLa cells. *Science* 194: 431-3.
- 877
- 878 107. Darzacq X, Shav-Tal Y, de Turris V, Brody Y, Shenoy SM, et al. (2007) In vivo dynamics of RNA polymerase II transcription. *Nat Struct Mol Biol* 14: 796-806.
- 879
- 880 108. Kos M, Tollervey D (2010) Yeast pre-rRNA processing and modification occur cotranscriptionally. *Mol Cell* 37: 809-20.
- 881
- 882 109. Darnell JE Jr (2013) Reflections on the history of pre-mRNA processing and highlights of current knowledge: a unified picture. *RNA* 19: 443-60.
- 883
- 884 110. Boström K, Wettsten M, Borén J, Bondjers G, Wiklund O, et al. (1986) Pulse-chase studies of the synthesis and intracellular transport of apolipoprotein B-100 in Hep G2 cells. *J Biol Chem* 261: 13800-6.
- 885
- 886
- 887 111. Meyers R, editor (2004) *Encyclopedia of Molecular Cell Biology and Molecular Medicine*, Volume 1, 2nd Edition. ISBN: 978-3-527-30543-8. Wiley-Blackwell.
- 888
- 889 112. Rosenbluth MJ, Lam WA, Fletcher DA (2006) Force microscopy of nonadherent cells: a comparison of leukemia cell deformability. *Biophys J* 90: 2994-3003.

**Table 1:** Myelomonocytic transcription factor connectivity used in the signal integration and phenotype modules.

Effector	Effect	Target	Source
RAR $\alpha$	+	RAR $\alpha$	(58)
	+	PU.1	(59)
	+	C/EBP $\alpha$	(36)
	+	IRF-1	(60)
	-	Oct4	(61)
	+	CD38	(62)
	+	p21	(63)
	+	AhR	(64)
	+	Egr-1	(65)
PPAR $\gamma$	+	C/EBP $\alpha$	(66)
	+	IRF-1	(67)
	+	Oct1	(68)
	-	AP-1	(69)
	-	E2F	(70)
	-	Egr-1	(71)
	+	CD38	(72)
	+	CD14	(73)
	+	p21	(74)
	-	p47Phox	(75)
PU.1	-	PPAR $\gamma$	(76)
	+	PU.1	(77)
	+	AP-1	(78)
	+	Egr-1	(32)
	+	CD11b	(79)
	+	p21	(80)
	+	p47Phox	(81)
C/EBP $\alpha$	+	PPAR $\gamma$	(66)
	+	PU.1	(37)
	+	C/EBP $\alpha$	(82)
	+	Gfi-1	(83)
	-	E2F	(84)
	+	CD14	(85)

891

	+	p21	(86)
IRF-1	+	CD38	(87)
	+	p21	(88)
	-	PU.1	(89)
	-	C/EBP $\alpha$	(90)
	-	E2F	(90)
	-	Egr-1	(32)
	-	p21	(90)
Oct1	+	PU.1	(91)
AP-1	-	PPAR $\gamma$	(69)
	+	PU.1	(92)
	+	p21	(93)
E2F	+	E2F	(94)
Egr-1	+	PPAR $\gamma$	(95)
	-	Gfi-1	(96)
	+	CD14	(97)
AhR	+	AP-1	(98)
	+	IRF-1	(99)
	-	Oct4	(100)
	-	PU.1	

**Table 2:** Characteristic model parameters estimated from literature.

Symbol	Description	Value	Units	Source
$R_1$	RNA polymerase abundance	85,000	copies/cell	(101, 102)
$R_2$	Ribosome abundance	$1 \times 10^6$	copies/cell	(103)
$G_i$	Characteristic gene abundance	2	copies/cell	this study
$K_X$	Saturation constant transcription	600	copies/cell	this study
$K_T$	Saturation constant translation	95,000	copies/cell	this study
$t_{1/2,m}$	characteristic mRNA half-life (transcription factor)	2-4	hr	(104)
$t_{1/2,p}$	characteristic protein half-life	10	hr	(105)
$\theta_{m,j}$	characteristic mRNA degradation constant	0.34	$hr^{-1}$	derived
$\theta_{p,j}$	characteristic protein degradation constant	0.07	$hr^{-1}$	derived
894				
$t_d$	HL-60 doubling time	19.5	hr	this study
$\mu$	growth rate	0.035	$hr^{-1}$	derived
$k_d$	death rate	$0.10\mu$	$hr^{-1}$	derived
$e_T$	elongation rate RNA polymerase	50-100	nt/s	(106–109)
$e_X$	elongation rate Ribosome	5	aa/s	(110)
$L_{T,o}$	characteristic gene length	15,000	nt	(111)
$L_{X,o}$	characteristic transcript length	5,000	nt	derived
$k_T$	characteristic transcription rate	1.44	$hr^{-1}$	derived
$k_X$	characteristic translation rate	3.60	$hr^{-1}$	derived
$D$	Diameter of an HL-60 cell	12.4	$\mu m^3$	(112)
$f_C$	cytoplasmic fraction	0.51	dimensionless	(112)

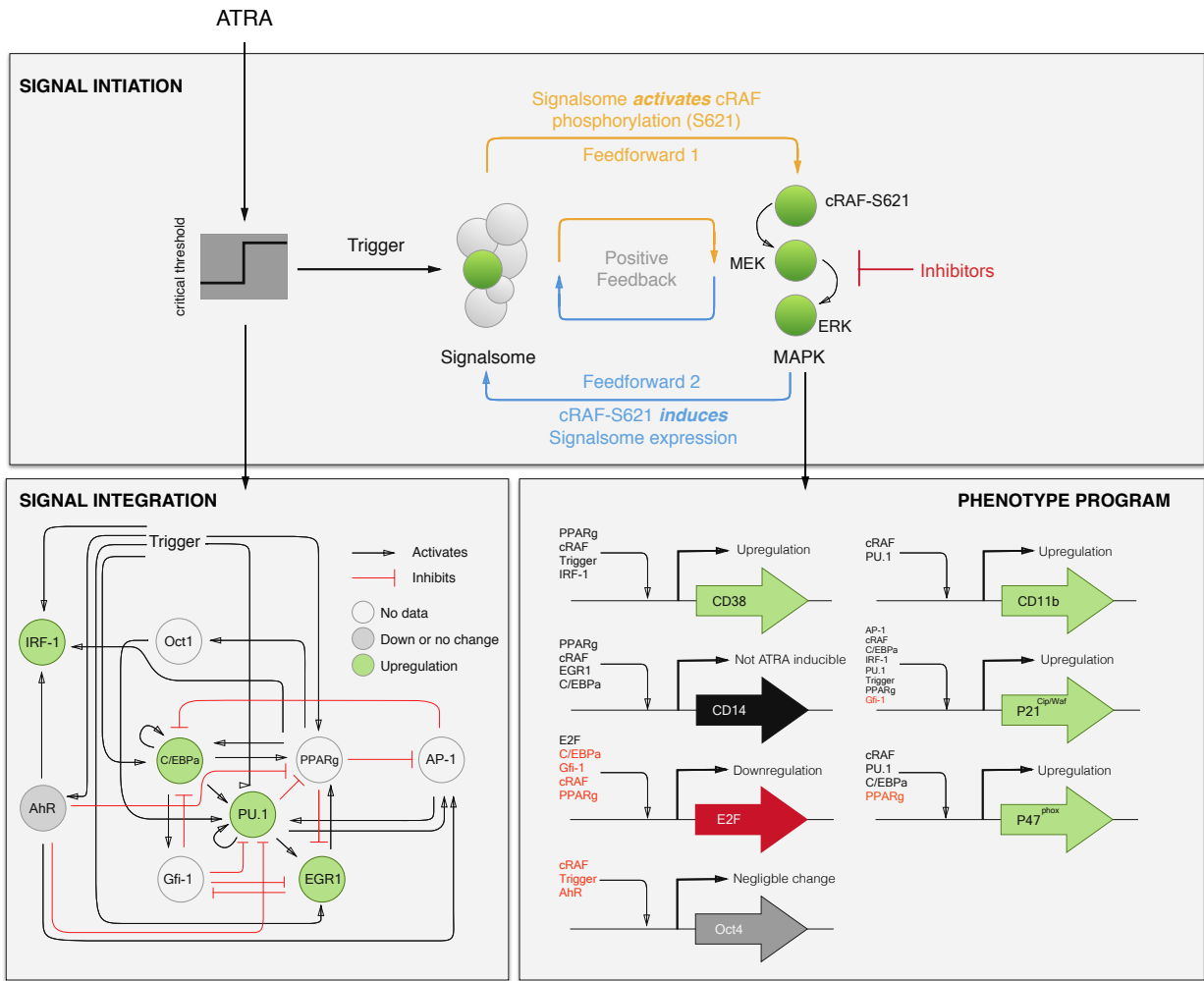


**Fig. 1:** Schematic of the effective ATRA differentiation circuit. Above a critical threshold, ATRA activates an upstream Trigger, which induces signalsome complex formation. Signalsome activates the mitogen-activated protein kinase (MAPK) cascade which in turn drives the differentiation program and signalsome formation. Both Trigger and activated cRaf-pS621 drive a phenotype gene expression program responsible for differentiation. Trigger activates the expression of a series of transcription factors which in combination with cRaf-pS621 result in phenotypic change.

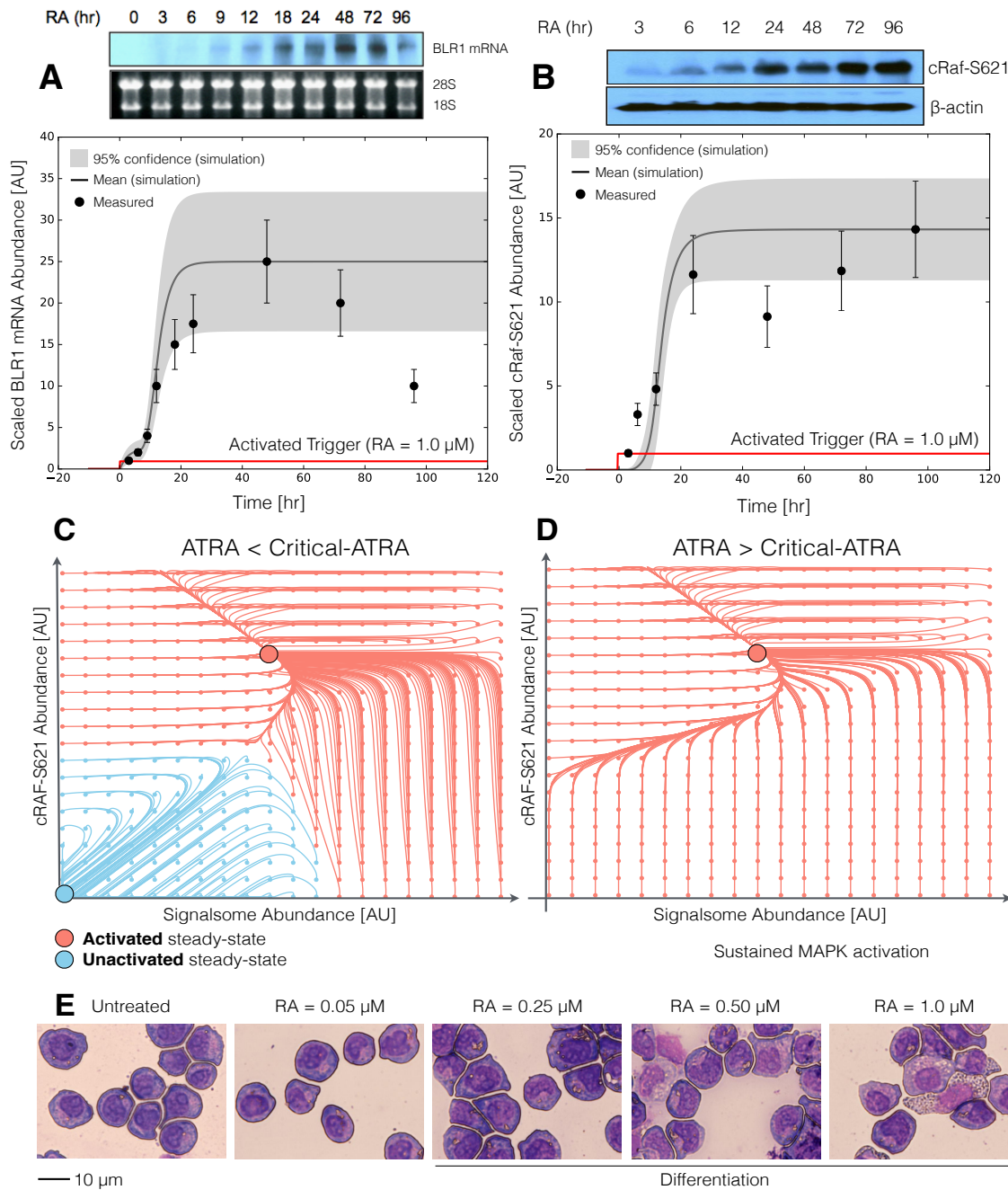


**Fig. 2:** Model analysis for ATRA-induced HL-60 differentiation. A: BLR1 mRNA versus time following exposure to  $1\mu\text{M}$  ATRA at  $t = 0$  hr. B: cRaf-pS621 versus time following exposure to  $1\mu\text{M}$  ATRA at  $t = 0$  hr. Points denote experimental measurements, solid lines denote the mean model performance. Shaded regions denote the 99% confidence interval calculated over the parameter ensemble. C: Signalsome and cRaf-pS621 nullclines for ATRA below the critical threshold. The model had two stable steady states and a single unstable state in this regime. D: Signalsome and cRaf-pS621 nullclines for ATRA above the critical threshold. In this regime the model had only a single stable steady state. E: Morphology of HL-60 as a function of ATRA concentration ( $t = 72$  hr).

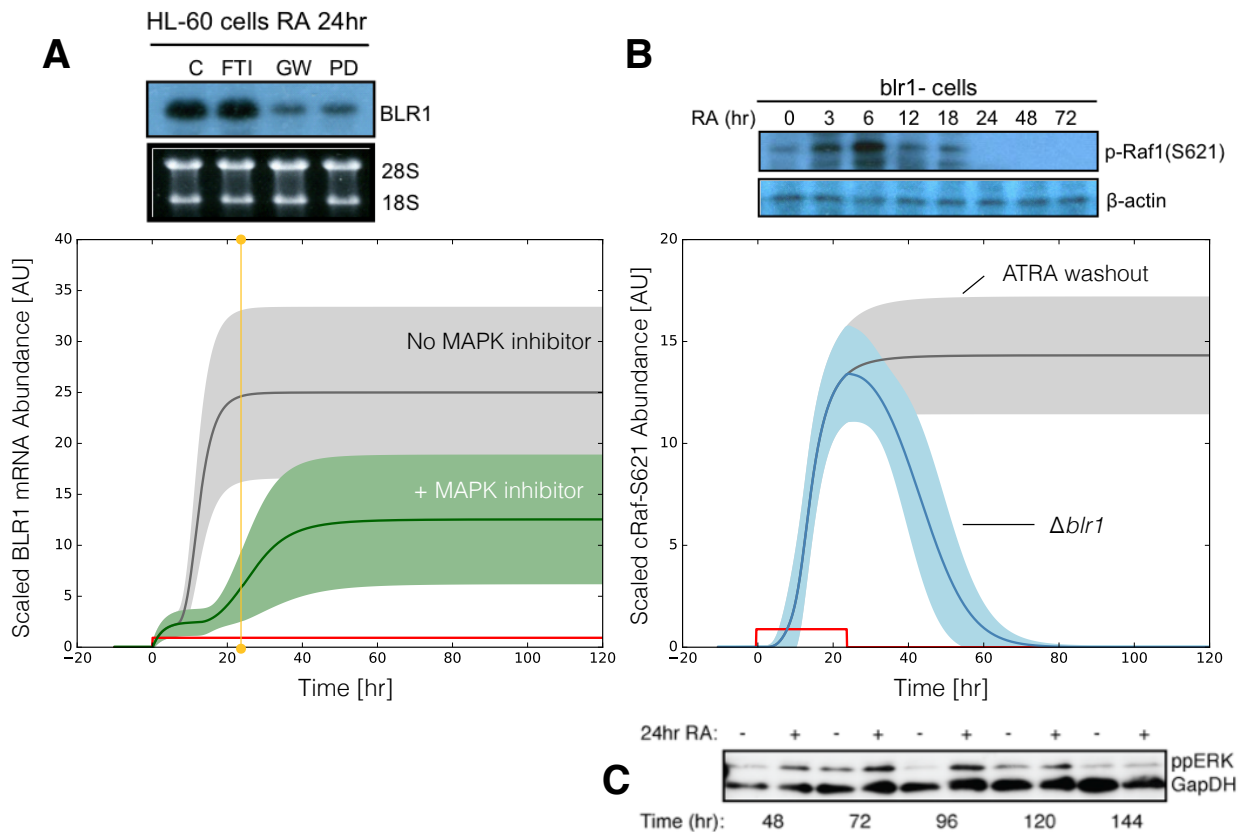


**Fig. 3:** Model simulation following exposure to  $1\mu\text{M}$  ATRA. A: BLR1 mRNA versus time with and without MAPK inhibitor. B: cRaf-pS621 versus time following pulsed exposure to  $1\mu\text{M}$  ATRA with and without BLR1. Solid lines denote the mean model performance, while shaded regions denote the 99% confidence interval calculated over the parameter ensemble. C: Western blot analysis of phosphorylated ERK1/2 in ATRA washout experiments. Experimental data in panels A and B were reproduced from Wang and Yen (20), data in panel C is reported in this study.

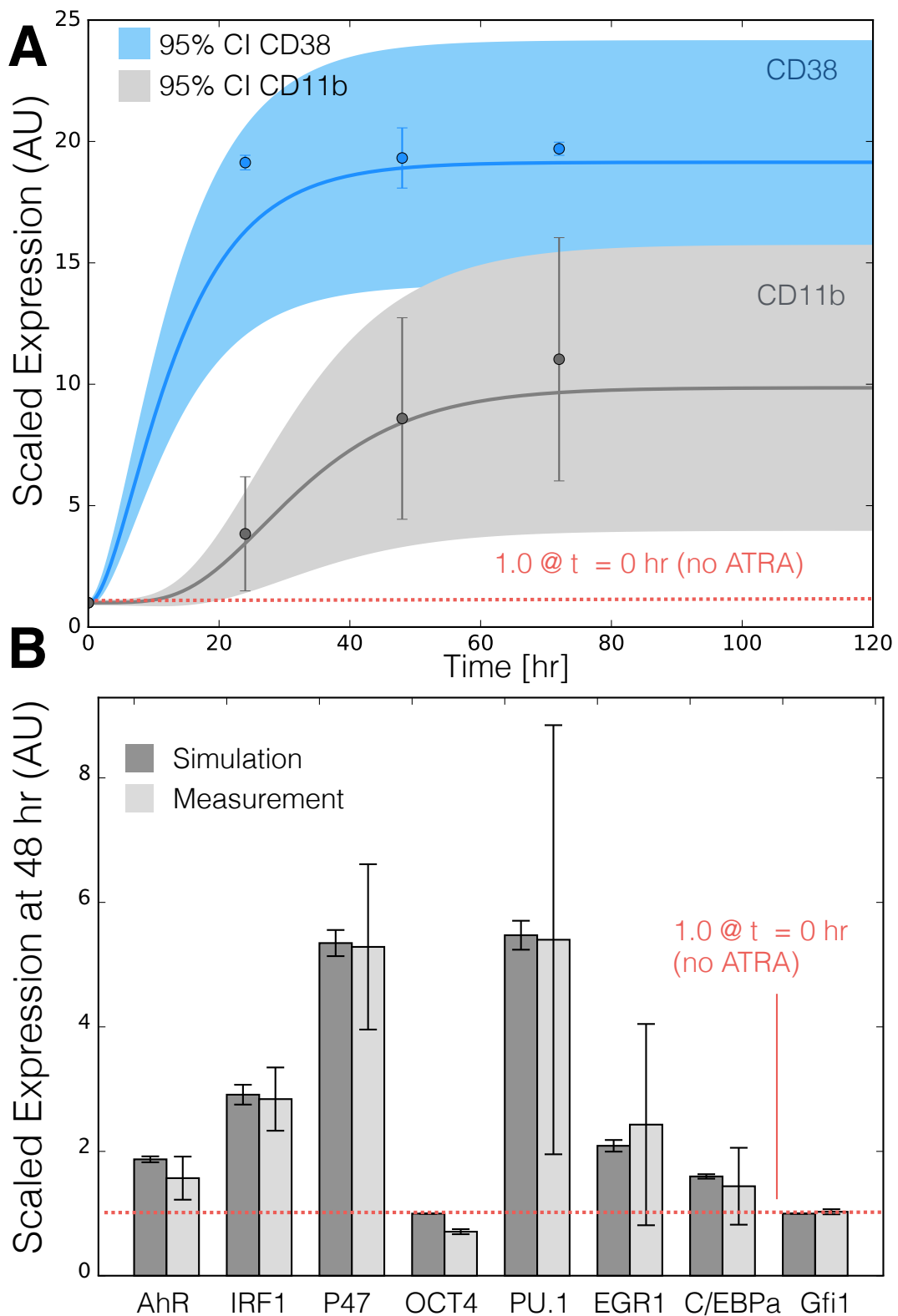


**Fig. 4:** Model simulation of the HL-60 gene expression program following exposure to  $1\mu\text{M}$  ATRA at  $t = 0$  hr. A: CD38 and CD11b expression versus time following ATRA exposure at time  $t = 0$  hr. B: Gene expression at  $t = 48$  hr following ATRA exposure. Experimental data in panels A and B were reproduced from Jensen et al. (25).

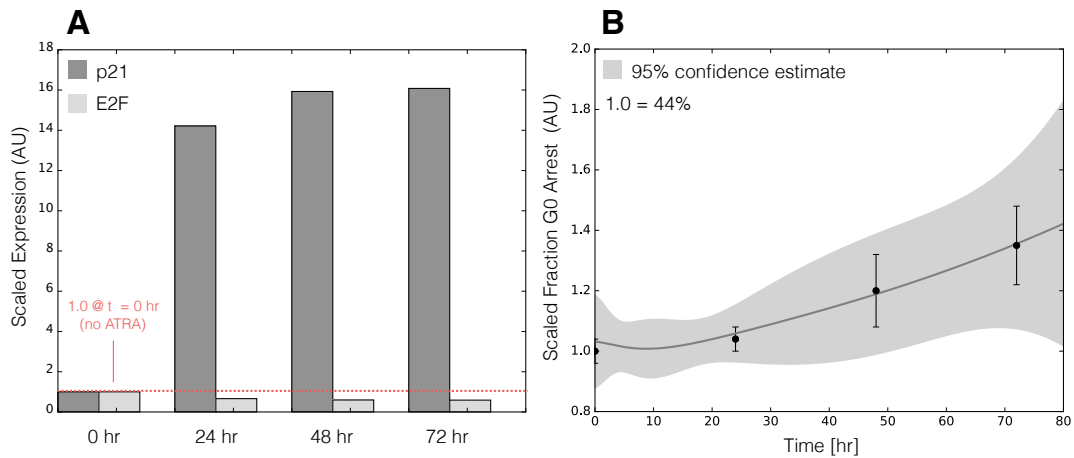


**Fig. 5:** Model simulation of HL-60 cell-cycle arrest following exposure to  $1\mu\text{M}$  ATRA at  $t = 0$  hr. A: Predicted p21 and E2F expression levels for the best parameter set following ATRA exposure at time  $t = 0$  hr. B: Estimated fraction of HL-60 cells in G0 arrest following ATRA exposure at time  $t = 0$  hr. The gray region denotes the 95% confidence estimate of the polynomial model. Experimental data in panel B was reproduced from Jensen et al. (25).

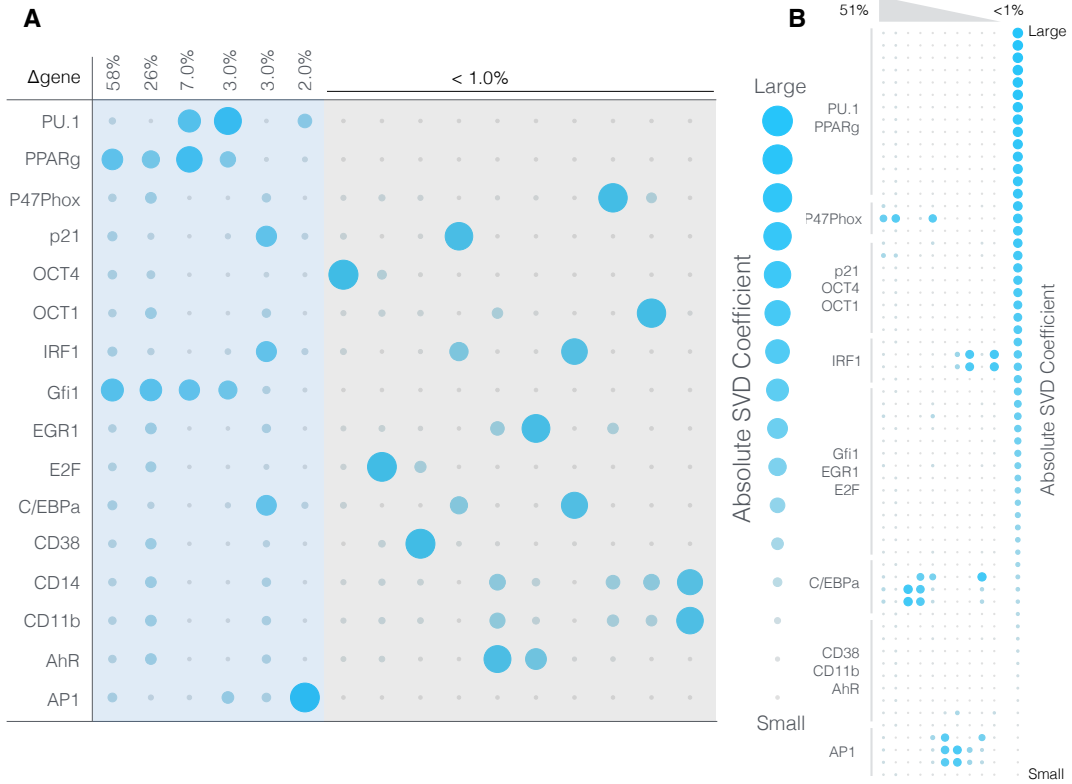


**Fig. 6:** Robustness of the HL-60 differentiation program following exposure to  $1\mu\text{M}$  ATRA at  $t = 0$  hr. A: Singular value decomposition of the system response ( $l^2$ -norm between the perturbed and nominal state) following pairwise gene knockout simulations using the best fit parameter set. The percentage at the top of each column describes the fraction of the variance in the system state captured by the node combinations in the rows. B: Singular value decomposition of the system response ( $l^2$ -norm between the perturbed and nominal state) following the pairwise removal of connections.

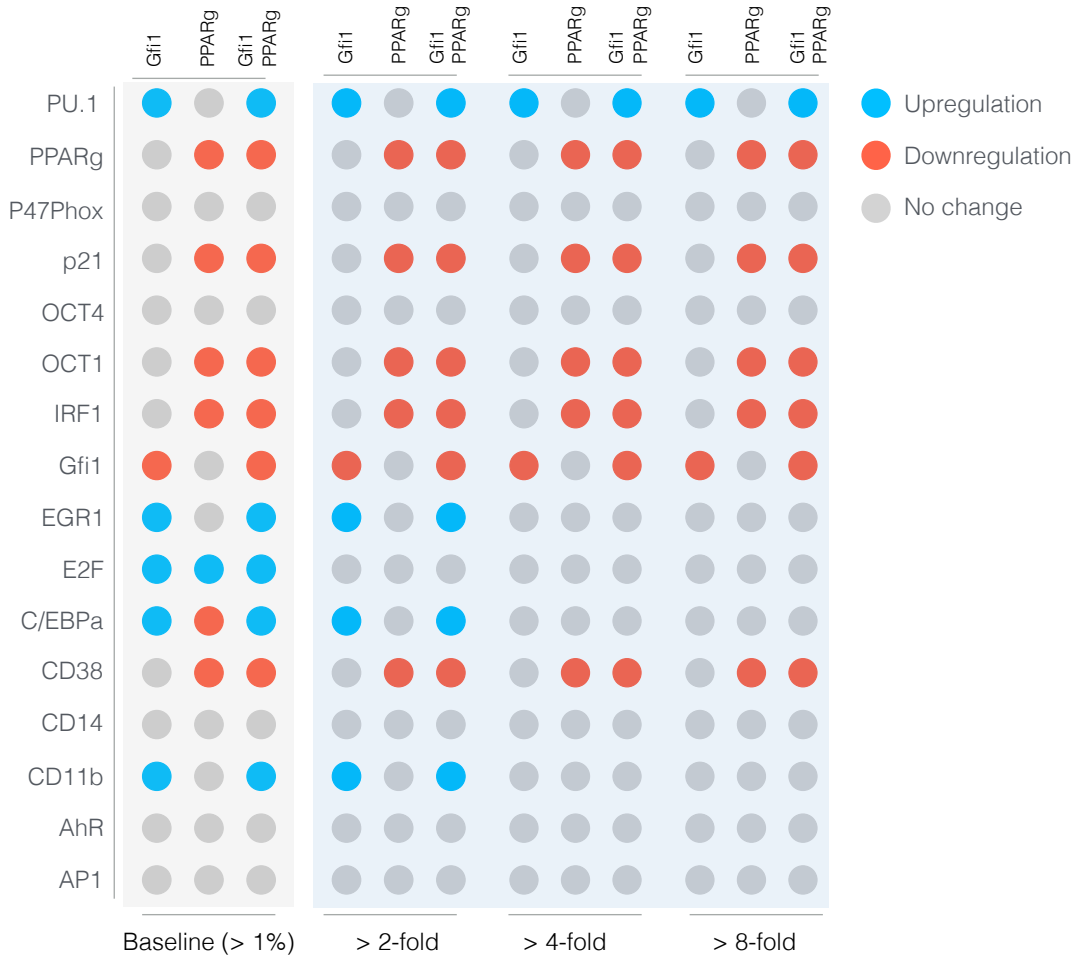


**Fig. 7:** Robustness of the HL-60 differentiation program following exposure to  $1\mu\text{M}$  ATRA at  $t = 0$  hr. Protein fold change at  $t = 48$  hr (rows) in single and double knock-out mutants (columns) relative to wild-type HL-60 cells. The responses were grouped into  $>2,4$  and  $8$  fold changes. The best fit parameter set was used to calculate the protein fold change.

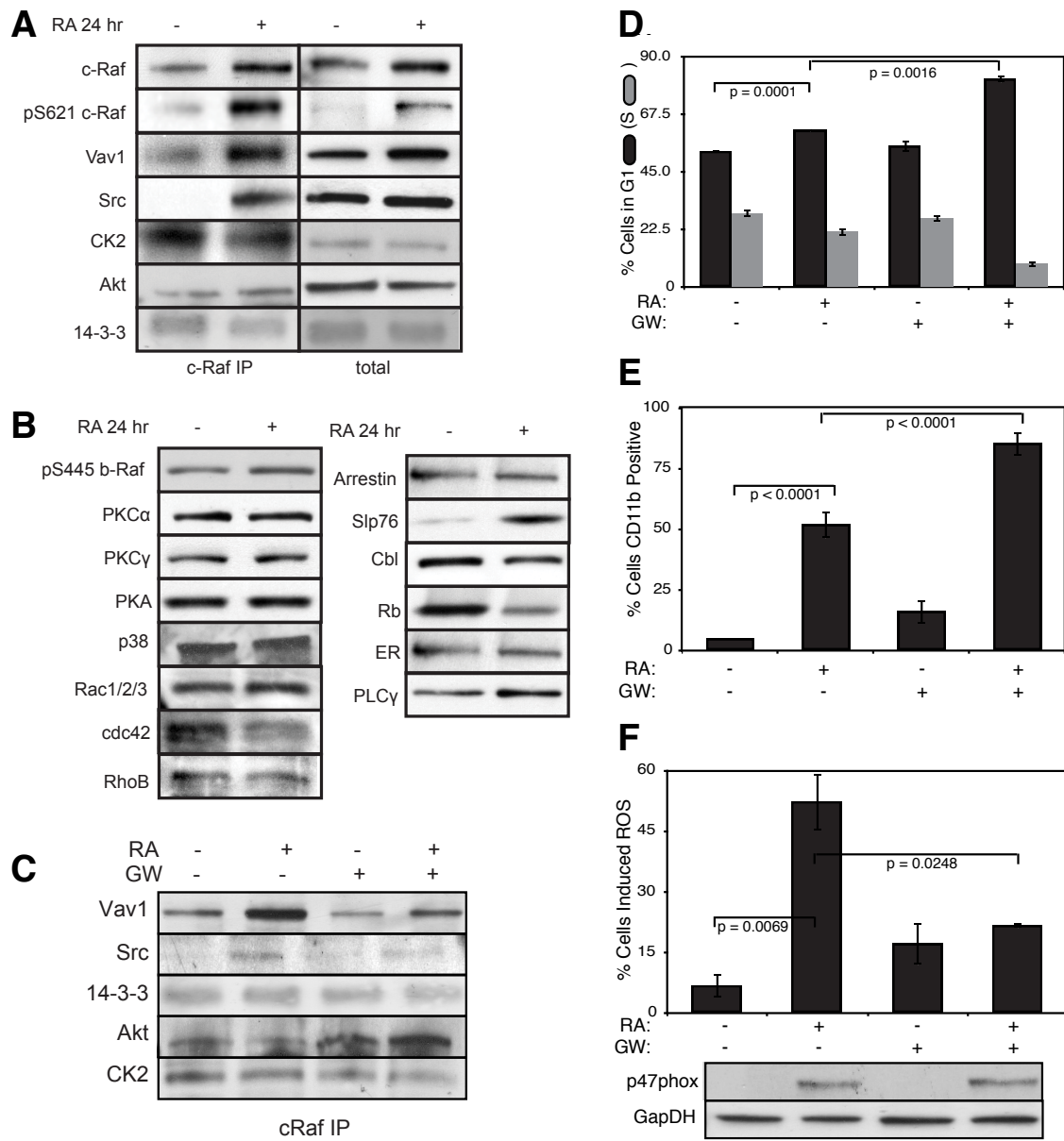


**Fig. 8:** Investigation of a panel of possible Raf interaction partners in the presence and absence of ATRA. A: Species identified to precipitate out with Raf: first column shows Western blot analysis on total Raf immunoprecipitation with and without 24 hr ATRA treatment and the second on total lysate. B: The expression of species considered that did not precipitate out with Raf at levels detectable by Western blot analysis on total lysate. C: Effect of the Raf inhibitor GW5074 on Raf interactions as determined by Western blot analysis of total Raf immunoprecipitation. The Authors note the signal associated with Src was found to be weak. D: Cell Cycle distribution as determined by flow cytometry indicated arrest induced by ATRA, which was increased by the addition of GW5074. E: Expression of the cell surface marker CD11b as determined by flow cytometry indicated increased expression induced by ATRA, which was enhanced by the addition of GW5074. F: Inducible reactive oxygen species (ROS) as determined by DCF flow cytometry. The functional differentiation response of ATRA treated cells was mitigated by GW5074.